The Rac1-PAK1-Arp2/3 signaling axis regulates CHIKV nsP1-induced filopodia and optimal viral genome replication

Olivier Aïqui-Reboul-Paviet, William Bakhache, Eric Bernard, Lise Holsteyn, Aymeric Neyret, Laurence Briant

Rac1-PAK1-Arp2/3 signaling axis regulates CHIKV nsP1-induced filopodia and optimal viral genome replication

Olivier Aïqui-Reboul-Paviet[#], William Bakhache[#*], Eric Bernard, Lise Holsteyn, Aymeric Neyret, Laurence Briant[$].

RNA Viruses and Metabolism Team, IRIM-CNRS UMR9004, Montpellier, 1919 route de Mende, 34293 Montpellier, France

[#] Contributed equally to the work

[$] Corresponding author

[*]Current address: Quantitative Virology and Evolution Unit, NIH-NIAID, Bethesda, MD

Running Title: Rac1 signaling axis in CHIKV nsP1 membrane deformation

Keywords: Chikungunya virus, nsP1, non-structural protein 1, Alphavirus, membrane rearrangement, cytoskeleton, cell signaling, genome replication

Abstract

Alphavirus infection induces dramatic remodeling of host cellular membranes, producing filopodia-like and intercellular extensions. The formation of filopodia-like extensions has been primarily assigned to the replication protein nsP1, which binds and reshapes the host plasma membrane when expressed alone. While reported decades ago, the molecular mechanisms behind nsP1 membrane deformation remain unknown. Using mammalian epithelial cells and Chikungunya virus (CHIKV) as models, we characterized nsP1-induced membrane deformations as highly dynamic actin-rich lamellipodia and filopodia-like extensions. Through pharmacological inhibition and genetic invalidation, we identified the critical contribution of the Rac1 GTPase and its downstream effectors PAK1 and the actin nucleator Arp2 in nsP1-induced membrane deformation. An intact Rac1-PAK1-Arp2 signaling axis was also required for optimal CHIKV genome replication. Therefore, our results designate the Rac1-PAK1-Arp2 pathway as an essential signaling node for CHIKV infection and

establish a parallel requirement for host factors involved in nsP1-induced plasma membrane reshaping and assembly of a functional replication complex.

Importance

The alphavirus nsP1 protein dramatically remodels host cellular membranes, resulting in the formation of filopodia-like extensions. Although described decades ago, the molecular mechanisms controlling these membrane deformations and their functional importance remain elusive. Our study provides mechanistic insight, uncovering the critical role of the Rac1 GTPase, along with its downstream effectors PAK1 and the actin nucleator Arp2, in the nsP1-associated phenotype. Furthermore, we demonstrate that the Rac1-PAK1-Arp2 pathway is essential for optimal CHIKV genome replication. Our findings establish a parallel in the cellular mechanisms governing nsP1-induced plasma membrane reshaping and the production of a functional replication complex in infected cells.

Introduction

RNA viruses reconfigure and manipulate the cytoskeleton network of their host to optimize the different stages of the viral life cycle. This manipulation specifically facilitates the endocytosis or micropinocytosis of incoming viral particles. It also promotes genome replication and contributes to the assembly and egress of progeny. Additionally, it critically determines intracellular trafficking of viral components and transmission to neighboring cells (reviewed in (1)). Viral manipulation of the host cytoskeleton often manifests by forming highly dynamic actin-rich plasma-membrane extensions called filopodia and lamellipodia. Filopodia consist of 10-100 µm long finger-like plasma-membrane extensions containing tightly packed actin filaments cross-linked by fascin into a stiff structure with accumulated myosin at the tip (2, 3). The rate at which the protrusions form is determined by actin polymerization at the filament tip facilitated by a dense complex of actin-binding proteins consisting of formin, Enabled/vasodilator-stimulated phosphoprotein (Ena/VASP) polymerases, and Eps8 (epidermal growth factor receptor kinase substrate 8) (4–7). Filopodia extend at the leading edge of cells to promote motility and adhesion and serve as sensory probes or in establishing cell-to-cell contacts (3). Lamellipodia are broad, sheet-like membrane protrusions, typically 1–5 µm wide and 100–300 nm thick, enriched with a 2D network of short, branched actin filaments, also participating in cell motility, migration, and mechanosensing (8). Actin filaments contained in both extension types are regulated by small guanosine triphosphatases (GTPases) in the Rho superfamily (9). These small monomeric proteins that include at least 20 members fluctuate between inactive and active states depending on guanosine diphosphate (GDP) or guanosine triphosphate (GTP) binding. In an active state, Rho GTPases recruit and activate downstream effector molecules at the plasma membrane, regulating actin nucleators and elongators (10). RhoA (Ras homolog family member), Cdc42 (cell division control protein 42), and Rac1 (Ras-Related C3 Botulinum Toxin Substrate 1) are the best-characterized GTPases contributing to actin organization during membrane reshaping (11, 12). RhoA activation cascade involves the downstream Rho-

associated protein kinase (ROCK) to regulate actin polymerization at the front of lamellipodia. However, it is also active in focal adhesion and stress fiber assembly (13, 14). Rac1 and Cdc42 regulate both distinct and shared effectors – the Neuronal Wiskott-Aldrich Syndrome protein (N-WASP) for Cdc42, the WASP family Verprolin homolog (WAVE) complex for Rac1 and IRSp53 and the serine/threonine kinase PAK1 (p21-activated kinase) for Rac1 and Cdc42). These effectors converge on the activation of the actin-related protein 2/3 (ARP2/3) complex, which controls the polymerization and dynamics of actin filaments (12, 15). Functionally, actin polymerization involved in membrane ruffles and lamellipodia is primarily regulated by both Rac1 and Cdc42 pathways. Cdc42 and associated signaling are the primary mediator of filopodium extension (3, 9, 11). Nevertheless, there is significant cross-talk between Rac1 and Cdc42 GTPases, and filopodia can form in the absence of Cdc42, protruding from the actin network of growing lamellipodia (16, 17).

As with other viruses, Alphaviruses dramatically reshape the cytoskeleton of their host, resulting in the formation of filopodia-like extensions (18–20). This family of mosquito-borne viruses includes Chikungunya virus (CHIKV), which rapidly spread in the mid-2000s, highlighting the significant impact these viruses can have on human health and the economy (21). CHIKV is transmitted to humans through the bite of infected *Aedes* sp. Mosquitoes, causing a febrile illness with debilitating joint pain that can last for months (22). At the cellular level, CHIKV infection begins with the intracytoplasmic release of its single-stranded, positive sense RNA genome of approximately 12 kb in length. This genome is divided into two ORFs encoding for four nonstructural proteins (nsP1, nsP2, nsP3, and nsP4), two envelope glycoproteins (E1 and E2), one capsid protein (C), and three peptides (E3, 6K and the transframe protein TF) (23). Translation of the 5’ ORF in the incoming genome results in the accumulation of two nonstructural polyproteins, P123 and P1234, which are sequentially processed by the nsP2 protease to release the viral enzymes: nsP1, the viral methyl/guanylyl transferase involved in RNA capping; nsP2 that also displays helicase and NTPase activities; nsP3, mainly involved in interaction with cellular cofactors, and nsP4, the viral RNA-dependent RNA polymerase that catalyzes the synthesis of viral RNAs (24–26). These mature

nonstructural proteins assemble to form the viral replicase, an essential unit for viral genome replication, located in the cytoplasmic face of plasma membrane-derived replication organelles, referred to as spherules (27–29). Within these organelles, identified as specialized sites of genome replication, nsP1 assembles into a dodecameric pore connecting the spherule to the cytoplasm. This pore not ony serves as a scaffold for the assembly of the replication complex assembly but also caps the 5'-terminus of newly synthesized RNA extruded into the cytoplasm (27, 28, 30). Structurally, nsP1 in this ring interacts with lipid bilayers through a central membrane-binding domain consisting of a stretch of palmitoylated cysteines conserved across Alphaviruses (27, 31, 32). In infected cells, this motif targets the viral replication complex to cholesterol-rich membrane microdomains, which is essential for genome replication (19, 20, 33–35). Additionally, palmitoylated cysteines also determine nsP1's capacity to dramatically reshape cell membranes into extensions (19, 20, 35, 36). Currently, the cellular machinery contributing to nsP1's membrane reshaping capacity has not been elucidated, and the functional significance of the resulting extensions reported decades ago is unknown. Thus, this nsP1-associated phenotype remains one of the most enigmatic characteristics of Alphavirus infection.

To adress this gap in knowledge, we investigated nsP1-induced cell deformations and questioned the direct contribution of cytoskeleton regulatory pathways. Our observations defined nsP1-induced cell extensions as highly dynamic lamellipodia and thin membrane extensions positive for actin, and VASP, Eps8, and fascin filopodia markers. The biogenesis of these filopodia-like protrusions was directed by the actin cytoskeleton network independently of microtubule involvement. Using drug perturbation experiments and genetic invalidation with siRNAs, we decipher the direct contribution of the main Rho GTPases in nsP1-associated phenotype. Our findings underscore the crucial role of Rac1 in nsP1-induced membrane deformations, while also pinpointing PAK1 serine-threonine kinase and Arp2 in the Arp2/3 actin nucleating complex as downstream effectors in cytoskeleton manipulation and membrane remodeling by nsP1. Furthermore, our investigation into the functional role of the Rac1-PAK1-Arp2 pathway in the CHIKV infectious cycle,

revealed its critical importance in viral genome replication. Overall, our data identify the Rac1-PAK1-Arp2 pathway as a critical player in nsP1-induced filopodia formation. Additionally, they underscore the parallell necessity of Rac1 signaling pathway for nsP1-associated membrane deformation and optimal genome replication.

Results

CHIKV nsP1 induces the formation of highly dynamic lamellipodia and filopodia-like extensions depending on conserved palmitoylated cysteines.

Alphavirus-infected cells are characterized by the formation of cell extensions (32, 37, 38). We first revisited this capacity for CHIKV in human epithelial cells. HEK293T, and HeLa cells were infected with CHIKV-377-mCherry reporter virus derived from the BNI-CHIKV 899 isolate, which encodes mCherry fused to nsP3, at a multiplicity of infection (MOI) of 3 for 16 hrs. In all cells tested, CHIKV infection resulted in dramatic membrane reshaping (Figure 1A). Compared to uninfected controls, CHIKV-positive cells exhibited an unusual number of plasma membrane protrusions resembling lamellipodia and filopodia (shown for HEK293T in Figure 1A). Interestingly, immunofluorescence studies revealed the accumulation of nsP1 at the plasma membrane bordering these extensions and sometimes at the tip, suggesting its contribution to virus-induced membrane remodeling. Considering other viral components, the nsP1 signal occasionally overlapped with nsP3 protein fluorescence and with double-stranded RNA (dsRNA), a replication intermediate, indicating the presence of active CHIKV replication complexes assembled on membranes bordering these extensions (Figure 1A, inset). This observation was reminiscent of our cryo-electron microscopy analysis of CHIKV-infected cells (J. Girard, O. Le-Bihan et al. https://doi.org/10.1101/2023.02.25.530016). A comparable profile of membrane reshaping was observed upon ectopic expression of the CHIKV nsP1 protein in HEK293T cells (Figure 1B) and in HeLa cells (Figure 2). Remarkably, similar morphological changes were observed when nsP1 was expressed in its native form or when fused with a fluorescent protein at either its C-terminus (nsP1-DsRed) or

N-terminus (GFP-nsP1) (Figure 1B). Upon ectopic expression, these different nsP1 proteins accumulated at the plasma membrane and in discrete intracytoplasmic compartments promoting highly dynamic morphological changes. Time-lapse video microscopy revealed at least two types of events at the plasma membrane. Firstly, we observed filopodia-like extensions that rarely exceeded 10 µm in length, rapidly growing and retracting from the body of the transfected cell (Figure 1C). Secondly, we frequently observed the formation of lamellipodia-like protrusions followed by retraction, resulting in the persistence of thin cell extensions tightly associated with the substrate (Figure 1D, red arrows). Thin extensions and lamellipodia deformations were simultaneously observed from the same cell, with filopodia sometimes extending from the lamellipodium (Figure 1D; white arrows). These phenotypes were significantly reduced in cells expressing an nsP1 mutant, referred to as $nsP1_{AAA}$, in which the triplet of palmitoylated cysteines at position 418-420 in the nsP1 membrane binding domain was replaced with a triplet of alanines (Figure 1B). In these cells, the filopodia number per cell quantified using the FIJI software was markedly lower than observed for the wild-type nsP1 (Figure 1E). Moreover, the length of the remaining extensions was significantly decreased when compared to cells expressing the wild-type GFP-nsP1 (Figure 1F). Nevertheless, this mutant still promoted the formation of a small number of filopodia compared with GFP-expressing cells, suggesting that palmitoylation is not the only determinant of nsP1-induced filopodia extensions.

Conservation of nsP1-induced membrane deformation capacity across alphavirus evolution.

Alphaviruses are classified into two monophyletic groups based on their geographical distribution and clinical manifestations in humans (39). CHIKV, Semliki Forest virus (SFV), and Sindbis virus (SINV) belong to the Old World viruses that typically causing arthritis symptoms. In contrast, New World alphaviruses like Venezuelan equine encephalitis virus (VEEV) manifest with neurological symptoms. Despite sharing at least 40% sequence identity, these two groups have evolved distinct virus-host interactions to replicate efficiently (40, 41). To investigate the conservation of nsP1 phenotype across

alphavirus evolution, the nsP1 coding sequence from SFV (SFV6 strain), SINV (AR339 strain), or VEEV (TC-83 strain) were cloned in-frame with GFP and transfected in HeLa cells. 24 hrs after transfection, confocal microscopy revealed, akin to CHIKV, a dramatic induction of cell protrusions comprising lamellipodia- and filopodia-like deformations (Figure 2A). However, a quantitative analysis of filopodia count showed that VEEV nsP1 induced significantly fewer filopodia per cell compared to CHIKV, SFV, and SINV (Figure 2B). We also explored whether nsP1 from Eilat virus (EO329 isolate), an alphavirus restricted to mosquito cells could induce membrane deformations in human cells. We observed that Eilat nsP1 did not significantly promote cell membrane protrusions compared to the control condition. Previous studies have linked membrane deformation ability to conserved cysteine residues covalently modified by palmitoylation in nsP1's central domain (18, 19, 35, 36, 42). Amino acid sequence comparison showed that EILV nsP1 possesses a unique cysteine at the corresponding position, similar to SINV (Figure 2C). Since EILV is arthropod-specific, our observation prompts the necessity to reinvestigate EILV nsP1's palmitoylation and membrane deformation capacity in mosquito cells. With this exception, nsP1's capacity to reshape cell membranes appears to be a common feature of human-infecting alphaviruses, resulting in the formation of highly dynamic filopodia- and lamellipodia-like structures.

nsP1-induced membrane reshaping is mediated by the actin cytoskeleton.

Morphological and mechanical changes at the plasma membrane are orchestrated by the coordinated activities of microtubules, actin filaments, and stress fibers comprising the cytoskeleton. We investigated their respective contribution in nsP1-induced reshaping of HeLa cell membranes. Actin was visualized by transfecting the CMV-LifeAct-TagRFP plasmid, which expresses a fluorescent peptide staining filamentous actin structures in eukaryotic cells without disrupting actin dynamics (43). Co-transfection with GFP-nsP1, resulted in significant changes in the actin network compared to control cells that express the GFP protein (Figure 3A). Stress fibers were notably reduced, and actin appeared largely disorganized, while cortical actin beneath the plasma membrane remained largely

intact. Interestingly, nsP1 fluorescence frequently colocalized with actin signal, overlapping in cytoplasmic foci or along cytoplasmic filaments proximal to the plasma membrane. This filamentous colocalization of nsP1 with actin was particularly evident along filopodia-like structures and in the form of fibers in lamellipodia-like processes emerging from the cell body of transfected cells. Quantitative analysis of this colocalization, performed by calculating Pearson's coefficient, yielded an average value of 0.743± 0.096 across 95 regions of interest in 9 cells (Figure 3C). These observations suggest a direct crosstalk between nsP1 and the actin cytoskeleton. Contrasting with this result, the tubulin network, detected with an antibody that recognizes β-tubulin, was not perturbed in nsP1-expressing cells (Figure 3B). Moreover, nsP1-induced cell extensions were negative for β-tubulin signal with an average Pearson's correlation coefficient of 0,194±0.159, determined across 95 cell regions of interest in 11 cells (Figure 3C)). In light of these observations, actin fluorescence was tracked through live-video confocal microscopy to assess its re-distribution during nsP1-induced membrane protrusion formation. Time-lapse series were carried out using cells that co-express GFP-nsP1 and LifeAct-TagRFP. Intense actin filaments were observed at the base of and along growing filopodia-like protrusions (frame at 0 sec) and also in lamellipodia-like structures that were also positive for nsP1 signal (Figure 3D, frame at 90 sec). To assess the functional role of actin filaments and microtubules in nsP1-induced filamentous projections, we utilized cytochalasin D and nocodazole depolymerization agents acting on actin and microtubules, respectively. Non-toxic concentrations of these drugs were determined and added to cells 16 hrs after transfection with a GFP-nsP1 expression plasmid. Under these conditions, cytochalasin D potently reduced the number of extensions per cell compared with mock-treated condition (Figure 3E and 3F). In contrast, nocodazole less dramatically decreased the number of cell extensions per cell.

Characterization of nsP1-induced cell extensions.

Filopodia are typically characterized by the presence of actin filaments cross-linked by fascin into a stiff structure (44), along with the presence of a regulatory complex at their tip composed of VASP

and Eps8 that accelerates actin filament growth (4–7). To delve deeper into the nature of nsP1-induced cell extensions, we investigated the co-localization of the previously mentioned filopodia markers with membrane deformations. Cells were co-transfected to express a non-tagged nsP1 and GFP-fused Fascin, Eps8, or VASP. Confocal imaging of the cells revealed enrichment of Eps8, VASP, and fascin in nsP1-positive cell extensions (Figure 4A). While fascin was detected along the cell extensions, Eps8 protein was concentrated at the tip of these processes. Interestingly, in many instances, this signal colocalized with nsP1-enriched foci, as evidenced by the calculation of Pearson's correlation coefficient (Figure 4B). VASP was also detected in these extensions but did not consistently localize to the growing extremity, contrary to conventional filopodia (5, 6). Instead, VASP primarily concentrated at the base of filopodia and was also detected along the cell extension, exhibiting a profile very similar to fascin. These findings, therefore, identify CHIKV nsP1-induced cell extensions as actin-rich processes containing canonical filopodia markers but lacking VASP accumulation at the tip. Together with nsP1 localization at filopodia extremities, this suggests the involvement of an unconventional assembly mechanism.

Functional Rac1 GTPase is critical for nsP1-induced cell extension.

The actin cascades essential for filopodia formation are primarily initiated by Rho, Rac, and Cdc42 GTPases (Figure 5A) (45). We questioned the contribution of these GTPases in nsP1-induced cell extensions by employing pharmacological inhibitors. HeLa cells expressing the GFP-nsP1 protein were treated with NSC23766, ML141, or Y27632 inhibitors, selectively targeting Rac1, Cdc42, or ROCK (a downstream effector of RhoA), respectively (46–48). Drugs were added to cells 4 hrs post-transfection to prevent any inhibition of nsP1 transgene expression. The absence of drug toxicity was controlled in parallel (not shown). After an additional 20 hrs in culture, we quantified the number and length of plasma membrane extensions. GFP-nsP1 fluorescence level was detected in all conditions at a level equivalent to that observed in mock-treated cells (Figure 5B). Our quantitative analysis revealed that the number and length distribution of filopodia formed in the presence of

ML141 and Y-27632 were comparable to that assembled in the control condition. However, the number of filopodia per cell was slightly more heterogeneous in the presence of Y-27632 (Figure 5B and 5C). In contrast, a significant reduction in filopodia count was observed in cells treated with NSC23766, which specifically prevents the conversion of the inactive Rac1-GDP to active Rac1-GTP (46) compared with the mock-treated culture. Filopodia formed under this condition were shorter than in mock-treated cells (Figure 5D). To confirm the possible regulatory role of Rac1 in nsP1-induced membrane deformation and to avoid off-target drug effects, similar experiments were conducted in cells transfected with Rac1 siRNA or non-targeting controls before transfection of the GFP-nsP1 plasmid. Reduced Rac1 expression was confirmed by immunoblot (Figure 5E). Filopodia count analysis revealed that these cells displayed significantly fewer membrane extensions than control cells (Figure 5F and 5G). As observed in the presence of NSC23766, the remaining extensions were shorter than in cells transfected with non-targeting siRNA (Figure 5H). Finally, we confirmed the requirement of Rac1 GTPase activity in nsP1-associated phenotype by co-transfecting plasmids encoding the untagged nsP1 with plasmids encoding either a Rac1 dominant negative mutant (Rac_{N17}) or a wild-type Rac1 (Rac_{WT}) fused with GFP. Cells expressing the green fluorescence were investigated for cell membrane deformations. As depicted in Figure 5I, expression of the Rac1-N17 mutant impaired the formation of nsP1-induced cell extensions compared to cells expressing the wild-type Rac1 GTPase. Overall, these results underscore the necessity of a functional Rac1 protein for the production and growth of actin-containing nsP1-induced filopodia-like extensions.

Characterization of Rac1 downstream effectors.

In its GTP-bound form, activated Rac1 interacts with specific effectors to initiate many signaling cascades regulating cytoskeleton dynamics. Notably, Rac1 effector proteins such as p21 activating kinase (PAK1), insulin receptor substrate of 53 kDa (IRSp53), and IQ Motif Containing GTPase Activating Protein 1 (IQGAP), regulate the Arp2/3 actin polymerization complex (49). Additionally, Rac1 interacts with and activates phosphatidylinositol-4-phosphate 5-kinase (PIP5-kinase), a key

enzyme in the metabolism of phospholipids that promotes actin nucleation by the Arp2/3 complex (50). To decipher which pathway(s) may contribute to nsP1 activity in membrane deformation, Rac1 effectors were targeted with siRNA in HEK293T cells before transfection of the GFP-nsP1 plasmid and quantification of cell extensions. Decreased expression of the targeted protein was confirmed by Western blot analysis (Figure 6A). Our analysis revealed that nsP1-induced extensions formed less efficiently in cells with invalidated Rac1 effectors than in control cells (Figures 6B and 6C). Specifically, siRNA against PIP5K1, IRSP53, and IQGAP mildly reduced the number of nsP1-induced cell extensions per cell. However, a more pronounced reduction in filopodia number per cell was observed in cells transfected with siRNA against PAK1 (Figure 6C). Furthermore, PAK1 siRNA dramatically reduced the length of the remaining cell extensions (Figure 6D). Finally, we investigated the contribution of the downstream Arp2/3 actin polymerization complex to the nsP1-associated phenotype. siRNA transfection against Arp2 significantly reduced the number and length of GFP-nsP1-induced cell extensions compared to control cells (Figures 6C and 6D). These results collectively highlight the pivotal role of Rac1 in the formation of nsP1-induced cell extensions. While suggesting a potential redundant contribution of IRSp53, PIP5K1, and IQGAP in this phenotype, our observations designate PAK1 and Arp2 as major downstream effectors of nsP1-induced membrane deformation.

Role of the Rac1/PAK1/Arp2 signaling pathway in the CHIKV life cycle.

Filopodia formation induced by viruses from distinct families facilitates virus multiplication through diverse mechanisms (51, 52). After establishing the contribution of the Rac1/PAK1/Arp2 signaling axis in nsP1-induced cell extensions, we investigated its significance in CHIKV infection. Focusing on Rac1's pivotal role, we examined CHIKV infection in cells cultured with non-toxic concentrations of NSC23766. The cells were preincubated with the drug for 1 hr and then infected with a CHIKV-luciferase reporter virus (strain LR-OPY1) containing a luciferase gene in the C-terminus of nsP3 sequence, used at an MOI of 2.5 for 6 hrs. This time point corresponds to a single alphavirus replication cycle (53). Under these conditions, CHIKV infection, monitored by quantification of the

reporter-encoded luciferase in the cell lysates, was significantly reduced in NSC23766-treated cells (Figure 7A). This inhibitory effect was further confirmed by qRT-PCR measurement of intracellular genomic RNA over time (Figure 7B). In these experimental conditions, Y27632 and ML-141 also significantly decreased CHIKV infection when added to the cells before the virus challenge (Figure 7A). To further elucidate the proviral function of GTPases, we assessed their requirement for CHIKV intracellular replication. Since the CHIKV entry process is completed after 1h of viral challenge (53, 54), we investigated whether Rho GTPase inhibitors would retain their antiviral activity when added after this time point. Cells were infected with the CHIKV-luciferase reporter virus for 1 hr, after which the viral inoculum was removed and replaced with fresh medium supplemented with increasing concentrations of NSC23766 for 6 hrs, before quantification of CHIKV-encoded luciferase activity (Figure 7C). In these conditions, NSC23766 exhibited a potent dose-dependent inhibition on CHIKV intracellular replication, a result confirmed by quantification of CHIKV RNA genomes over time (Figure 7D). In contrast, Y27632 and ML-141 only marginally reduced CHIKV infection without any dose-dependent activity (Figure 7C). These observations suggest that Cdc42 and ROCK are mainly involved at the entry step of CHIKV, while Rac1 plays a central role in the intracellular replication of the virus.

In alphavirus-infected cells, nsP1 is integral to the viral replicase, where it orchestrates the bending of the plasma membrane, a crucial event in the biogenesis and maintenance of replication organelles hosting genome replication and transcription (27, 31). Given Rac1's implication in nsP1-mediated membrane deformation, we assessed its possible involvement in CHIKV genome replication as an indicator of spherules biogenesis and/or functionality. To this end, we utilized a CHIKV transreplication system that mimics the intracellular steps of the viral cycle. Plasmids encoding the CHIKV nsPs and a pseudogenome template, in which the coding sequences are replaced by luciferase reporter genes (55), were co-transfected into HEK293T cells. Six hrs post-transfection, the medium was supplemented with increasing concentrations of NSC2766. Quantification of genome replication, reflected by luciferase activity in the cell lysate, confirmed that the Rac1 inhibitor caused a dose-

dependent reduction in CHIKV genome replication (Figure 8A) without significantly affecting nsPs translation, as assessed by immunoblot analysis of nsP1 expression in the cell lysate (Figure 8B). This result was validated by transfecting the CHIKV transreplicon system into cells co-expressing either GFP-Rac1$_{N17}$ or GFP-Rac1$_{WT}$ constructs (Figure 8C). After 24 hrs, replicon activity was decreased by two-fold in cells expressing the dominant negative GFP-Rac1$_{N17}$ mutant compared to mock-transfected cells, while activity remained unchanged in cells expressing the GFP-Rac1$_{WT}$ protein. Similarly, transfection of Rac1-specific siRNA (siRac1) resulting in a 75 % loss in Rac1 expression decreased CHIKV genome replication by 70 % compared with the non-targeting siRNA (siCtrl) (Figure 8B). Given that Rac1 activity controls PAK1 and Arp2 previously identified as key effector in nsP1-induced membrane deformation, we investigated their requirement for CHIKV genome replication by cotransfecting the CHIKV transreplication system together with siRNA targeting PAK1 or Arp2 (Figures 8E and 8F). Decreased expression of PAK1 or Arp2 significantly reduced the activity of the transreplication system. These findings suggest that Rac1 and its downstream effectors PAK1 and Arp2, are essential for the CHIKV life cycle and genome replication. Therefore, the requirement for a functional Rac1-PAK1-Arp2 axis in CHIKV genome replication parallels the functional importance of this signaling axis for nsP1-induced membrane reshaping.

Discussion

Alphavirus infection of mammalian cells has been long reported to induce a profound reorganization of the host cell plasma membrane (56, 57). These morphological alterations manifest with the emergence of long-distance extracellular extensions (>10 μm), positive for α-tubulin and actin, specifically induced by the expression of the E2 envelope glycoprotein (37, 58, 59). Additionally, shorter tubulin-negative filamentous processes of approximately 2 to 7 μm in length have been observed during infection. This phenotype is recapitulated by the isolated expression of the viral methyl/guanylyltransferase nsP1 (42). Despite being described decades ago, nsP1-induced cell extensions were incompletely characterized. Moreover, the cellular machinery hijacked for their

304 production and their functional implication in the Alphavirus life cycle has remained poorly
305 understood. Therefore, this study was designed to address these gaps. Using mammalian epithelial
306 cells as a model, we confirm that CHIKV nsP1, expressed as an isolated protein, induces dramatic
307 reshaping of the cell plasma membrane, resulting in the growth of filopodia-like protrusions. We
308 report that nsP1 also promotes the production of lamellipodia-like structures, which retract, leaving
309 behind thin extensions attached to the culture substrate. Both events are highly dynamic, resulting in
310 the accumulation of actin-positive thin membrane processes at the plasma membrane. These
311 extensions are almost abolished by the actin-depolymerizing agent cytochalasin D. Interestingly,
312 despite the absence of tubulin in these cell extensions, the frequency of nsP1-induced cell
313 protrusions was reduced by half by using the tubulin inhibitor nocodazole, suggesting an
314 actin/microtubules crosstalk that warrants further investigations (60, 61). In this study, we focused
315 on actin regulators to provide a first mechanistic insight into nsP1-associated phenotype. Using
316 chemical and genetic invalidation strategies, we identified the Rac1 GTPase and its downstream
317 effectors PAK1 and Arp2 in the actin nucleator complex as key players in nsP1-induced membrane
318 deformations. Remarkably, we found that the Rac1-PAK1-Arp2 pathway is also critical for genome
319 replication, establishing a positive correlation between nsP1-induced plasma membrane reshaping
320 and functional replication complex formation.

321 Previous investigations on the nsP1-associated phenotype primarily focused on nsP1 sequence
322 determinants responsible for its deformation capacity. These studies have highlighted the critical
323 contribution, particularly in mammalian cells, of a central cysteine palmitoylation motif conserved
324 across alphavirus evolution (35, 36, 42, 62). In this study, we confirmed that the nsP1-associated
325 membrane deformation capacity is generally conserved across alphavirus evolution and requires the
326 presence of at least one conserved cysteine in its palmitoylation motif. However, despite bearing this
327 conserved determinant, VEEV nsP1 exhibited a limited ability to remodel the plasma membrane
328 compared to other Old World Alphavirus included in this study. Unexpectedly, we also observed that
329 EILV nsP1 scarcely deformed the membranes of human epithelial cells despite having a conserved

cysteine residue at the palmitoylation site. Differences in nsP1 membrane reshaping capacity in human and arthropod cells have been documented previously (62), suggesting host-dependent interaction of nsP1 with the plasma membrane. The incapacity of the mosquito-adapted EILV nsP1 to remodel the plasma membrane of human epithelial cells reported in this study parallels these differences. Additionally, EILV has been identified as a mosquito-restricted Alphavirus, unable to replicate its genome in human epithelial cells (63, 64). While the mechanisms underlying this restriction remain unclear, the unusual nsP1 phenotype observed in this study may be part of this mechanism.

Here, we provide the first detailed characterization of membrane deformations induced by CHIKV nsP1 in mammalian cells. We report that the isolated expression of nsP1 results in the formation of thin cell extensions positive for actin and actin-bundling proteins, fascin and Eps8. Notably, these markers differentiate filopodia from tubulin-containing tunneling nanotubes, which also appear as thin, elongated cell membrane extensions, and are frequently observed in viral infections (65, 66). Additionally, nsP1-associated processes stained positive for VASP, an actin polymerase that typically localizes at the filopodia tip to accelerate actin filament assembly and filopodia growth (66). Contrasting with this picture, VASP localization at the tip of nsP1-induced cell projections was not reproducibly detected; instead nsP1 frequently accumulated at these tips, suggesting that CHIKV nsP1 enables the production of unconventional filopodia-like extensions.

Filopodia formation in physiological conditions is mainly controlled by the activation of Cdc42 (3) and RhoA (67), which are involved in the polymerization of actin into linear filaments. However, in our experiments, neither Cdc42 nor RhoA significantly contributed to the nsP1-associated phenotype. Instead, we observed a significant decrease in nsP1-induced filopodia number and size, upon inhibition of Rac1 using NSC23766, expression of the $Rac1_{N17}$ mutant and Rac1-specific siRNA, establishing the critical contribution of Rac1 in this process. Similarly, we identified Rac1 downstream effectors PAK1 and Arp2, part of the Arp2/3 actin polymerization complex, as essential players in

nsP1-induced membrane extensions. Rac1 GTPase is a crucial regulator of the Arp2/3 complex, producing a branched cortical actin meshwork necessary for membrane ruffling, lamellipodia formation, and assembly of multimolecular focal complexes (9, 12). Nevertheless, Rac1, in cooperation with the Arp2/3 complex, is also involved in filopodia formation through the convergent actin fibers elongation model of branched actin (68). In this process, actin networks formed in lamellipodia are further extended by elongation factors, resulting in parallel actin fibers cross-linked by fascin. We observed that nsP1-induced filopodia not only protrude directly from the body of transfected cells but also frequently extend beyond the leading edge of lamellipodia. Therefore, Rac1's role in promoting nsP1-mediated filopodia assembly is compatible with a convergent elongation model of branched actin. Interestingly, Rac1 is a host cofactor for many different human viruses, contributing to morphological changes in infected cells. Among others, Rac1 controls filopodia formation in cells infected by Dengue virus, Human immunodeficiency virus, and Herpes Simplex virus (69–72). In Alphaviruses, Rac1 and Arp3, another constituent in the Arp2/3 complex, have been identified as cofactors in late infection (73). By controlling actin filament polymerization, they assist in trafficking of the E2 envelope glycoprotein to the cell surface. However, in contrast to this study, which involved PIP5K1α as an intermediate in this pathway, our results did not identify a critical role for this lipid kinase in the biogenesis of nsP1-induced filopodia. Instead, it designates the serine/threonine kinase PAK1, a well-known Rac1 downstream effector, as essential to this process. Thus, E2-induced late actin reorganization and nsP1-induced cell extensions likely mobilize distinct Rac1-controlled signaling pathways. Despite this converging evidence regarding Rac1 manipulation by Alphaviruses, the mechanisms by which this GTPase becomes activated, especially upon nsP1 expression, remains unresolved. Under physiological conditions, Rac1 activation is regulated by specific guanine nucleotide exchange factors (GEFs) acting as nodes for upstream signals (74). These GEFs interact with membrane-bound Rac1, converting the inactive GDP-bound Rac1 into an active GTP-bound state. Although Rac1 inhibition by NSC23766 and expression of a dominant negative Rac1-N_{17} mutant both prevented nsP1-mediated membrane deformation, direct evidence of Rac1

activation by nsP1 was not consistently observed in this study (not shown). Nonetheless, our recent findings regarding nsP1's affinity for cholesterol-enriched plasma membrane microdomain, where Rac1 also partitions (35, 75), suggest a possible crosstalk between these two proteins.

Having established the critical contribution of the Rac1-PAK1-Arp2 pathway in nsP1-induced filopodia processes, we examined its contribution to the CHIKV life cycle. We observed that Rac1, Cdc42, and RhoA GTPases are all essential for optimal infection of human epithelial cells. However, using a well-established CHIKV replicon system to assess intracellular replication steps, we found that only Rac1 invalidation decreased genome transcription/late translation without affecting intracellular nsPs expression. We established a similar contribution for PAK1 and Arp2 downstream effectors of Rac1. Altogether, our results identify RhoGTPases as CHIKV cofactors with variable contribution to early and intracellular replication steps, highlighting the crucial role of the actin-regulating Rac1-PAK1-Arp2 axis in genome replication. This model contrasts with the results of Radoshitzsky and colleagues (73), who used cells stably expressing a noncytotoxic, persistently replicating CHIKV mutant where Rac1 signaling was dispensable for genome replication (76). However, it corroborates our previous work demonstrating the essential requirement of actin dynamics for CHIKV post-entry events (54). Previous studies have suggested interactions between Alphavirus replicase and the actin network, based on the observation of replication complexes aligned with actin fibers in the cytoplasm of infected cells (77, 78) and the presence of high concentrations of actin in purified replication complexes (79, 80). Furthermore, the recent discovery of interactions between CHIKV nsP3 and the actin cytoskeleton rearranging protein CD2 associated protein (CD2AP), which are required for optimal infectivity, also supports the direct interplay between CHIKV replication machinery with actin (81). Our results highlight the need to further explore the relationships between actin-dependent membrane rearrangements induced by nsP1 and the mechanisms of viral genome replication. In the context of the relationship between nsP1 palmitoyl-dependent membrane affinity, filopodia formation, and viral infectivity (18, 82), our finding on the role of the Rac1/PAK1/Arp2 signaling axis

406 in both membrane deformations and viral replication opens new perspectives for understanding this
407 process.

408 **Material and Methods**

409 **Cell culture**: Human epithelial HEK293T cells (ATCC# CRL-3216), HeLa cells (ATCC# CCL-2), BHK21
410 cells (ATCC# CCL-10) used for propagation and Vero cells (ATCC# CCL-81) used for virus titration were
411 grown in Dulbecco's modified Eagle's medium (DMEM GlutaMAX, high glucose, Thermo Fisher
412 Scientific) supplemented with penicillin and 10% heat-inactivated fetal calf serum (FCS, Lonza). Cell
413 cultures were maintained at 37°C in a 5% CO2 atmosphere. In drug experiments, cell viability was
414 measured using Cell Titer 96 Aqueous one solution cell proliferation assay (Promega) following the
415 manufacturer's protocol.

416 **Viruses and infection:** Reporter viruses CHIKV-luc (LR2006_OPY1 strain) and CHIKV-m377 (BNI-CHIKV
417 899 isolate), containing respectively the renilla luciferase or the mCherry coding sequence inserted
418 into nsP3 sequence, have been described previously (76, 83). Virus stocks were produced and titered
419 using plaque assay as reported (35). Virus-encoded luciferase quantification was performed by lysing
420 the cells with Passive Lysis Buffer (Promega), followed by incubation with the Genofax C luciferase
421 reagent (Yelen Analytics). Luminescence was measured using a Spark 10M fluorometer (Tecan).
422 Values were normalized to protein content in the sample determined using the BCA Assay (Pierce).

423 **Plasmids transfection and siRNA knockdown:** CHIKV nsP1 expression plasmids were derived from
424 the CHIKV-LR-OPY1 (84) infectious clone. The GFP-nsP1 and GFP-nsP1$_{AAA}$ mutant were generated as
425 reported previously (35). The sequences coding for SFV (SFV6 strain), SINV (AR339 strain), VEEV (TC-
426 83 strain), or EILV (EO329 isolate), were PCR amplified the using primers shown in Table 1 and
427 subcloned into the peGFP-C1 plasmid. Plasmid encoding GFP-Eps8, GFP-VASP and GFP-fascin are gifts
428 from Andrea Disenza (IFOM Foundation, Institute FIRC of Molecular Oncology, Milan, Italy**)** (85).
429 Expression plasmids for GFP-Rac1$_{WT}$ and GFP-Rac1$_{N17}$ mutant were provided by Cécile Gauthier-

Rouvière. siRNA targeting Rac1, Arp2, PAK1, and the nontargeting control siRNA were purchased from Sigma-Aldrich. siRNA against IRSp53, IQGAP and PIP5K1 were from IDT (Table 1). Plasmids and siRNA (50nM) were transfected using JetPrime reagent according to the manufacturer's recommendations (Polyplus Transfection).

Drug treatment: The Rac1 inhibitor NSC23766 (N6-[2-[5-(Diethylamino)pentan-2-ylamino]-6-methyl-4-pyrimidinyl]-2methylquinoline-4,6-diamine), ML-141 (4-[4,5-Dihydro-5-(4-methoxyphenyl)-3-phenyl-1H-pyrazol-1-yl]benzenesulfonamide) an inhibitor of Cdc42, ROCK inhibitor Y27632 (1R,4r)-4-((R)-1-aminoethyl)-N-(pyridin-4-yl)cyclohexanecarboxamide), CK-666 (2-Fluoro-N-[2-(2-methyl-1H-indol-3-yl)ethyl]-benzamide) an inhibitor of the Arp2/3 complex, nocodazole, and cytochalasin D were purchased from Sigma Aldrich. IPA3 was obtained from MedChemExpress.

Antibodies: Antibodies against Rac1 (#ARC03) was purchased from Cytoskeleton. Rabbit polyclonal sera against PAK1 (#A301-260A), and Arp2 (#A305-216A-T) were from Bethyl. Anti-PIP5K1 (#67483-1) mAbs, anti-IRSp53 (#11087-2-AP from Proteintech), and anti-IQGAP (#22167-1-AP) were from Proteintech. Tubulin was detected using the 9F3 monoclonal antibody (Cell signaling technology) and dsRNA was revealed using the J2 monoclonal antibody (Scicons). Anti-nsP1 rabbit polyclonal serum was kindly provided by Pr Andres Merits (University of Tartu, Estonia). Anti-GAPDH (G8795) and anti-β actin (A3854) used in immunoblots were purchased from Sigma-Aldrich. Secondary reagents (anti-mouse and anti-rabbit antibodies conjugated with HRP, Alexa488, Alexa594, or Alexa647) were from (Invitrogen).

Microscopy and image analysis: Cells were grown on glass coverslips, washed with PBS and then fixed with 4% formalin (Sigma Aldrich) for 10 min at room temperature. Image acquisition was performed in bright field and GFP channel on an Axiovert Digital microscope (Carl Zeiss SAS, France) equipped with a 100X NA 1.4 oil-immersion objective (Zeiss). For confocal microscopy, the cells were permeabilized with 0.1% Triton X-100 in PBS and the nonspecific signal was blocked with 0.2% bovine

serum albumin, 0.05% Tween 20 in PBS. Incubation with primary antibody was performed for 2 hrs at room temperature. Secondary reagents were added for 1 h at room temperature, and nuclei were stained with 4',6-Diamidino-2-Phenylindole, dihydrochloride (DAPI; Sigma-Aldrich). After the final washes, coverslips were mounted with ProLong Gold Antifade mounting media (Thermo Fisher Scientific). Actin was labeled by transfection of CMV-LifeAct-TagRFP plasmid (43) into the cells. Images were acquired using a Leica SP5-SMD scanning confocal microscope equipped with a 63×, 1.4 numerical aperture Leica Apochromat oil lens at the Montpellier Resources Imaging platform. Image analysis was performed utilizing the ImageJ software and the JACoP plugin for Pearson's coefficient calculation considering region of interest after enhancement of signal-to-noise ratio.

Filopodia number Analysis: Optical sections of cells were imaged at 0.50 µm intervals from the bottom of the cell using a Leica SP5-SMD confocal microscopy system. For each image, 15–20 optical sections were taken, and the max projection of the stack was used for analysis. Filopodia numbers and lengths were determined using the FIJI software. Filopodia were only quantified along the periphery of cells. Filopodia was defined as >1 µm and grouped considering their size (<2 µm; 2-4µm; >4µm). The χ^2 test was used to assess difference in class distribution compared to the control sample.

CHIKV trans-replication assay: Plasmid encoding the nonstructural polyprotein from CHIKV was transfected into HEK293T cells with an equal amount of the HSPolI-Fluc-Gluc (55) plasmid, which encodes for a replication-competent CHIKV pseudogenome containing luciferase reporter sequences under the control of genomic and subgenomic promoters respectively. After 24 hrs in culture, the cells were washed in PBS and lysed using Passive Lysis Buffer (Promega). Expression of luciferase was determined using the Genofax A reagent and a Spark luminometer (Tecan). Reporter activities were normalized to the protein content in the sample, determined using the BCA Assay (Pierce).

Immunoblotting: Cells were incubated on ice in lysis buffer containing 50 mM Tris–HCl (pH 8.0), 100 mM NaCl, 1 mM MgCl2, 1% Triton X-100, and protease inhibitors (Complete; Roche). Lysates were clarified by centrifugation at 10,000 × g for 30 min and denatured by heating at 95°C for 5 min. Samples were separated by SDS-PAGE and then transferred to a polyvinylidene fluoride membrane (Hybond, Amersham). Membranes were blocked against nonspecific binding by using 0.5% casein, 0.1% Tween 20 in PBS, and incubated overnight at 4°C with primary antibodies. After wash steps with PBS containing 0.1% Tween 20, the membranes were probed with HRP-conjugated secondary antibodies for 1h at room temperature and then incubated with Luminata Forte (Merck). Chemiluminescence was detected using a ChemiDoc (Bio-Rad). Band intensity was determined with the ImageJ software, considering the GAPDH or actin signal as an internal control.

RT-qPCR quantification of viral genomes: Cells were lysed with the Luna® Cell Ready lysis module (New England Biolabs) according to manufacturer's instructions. One-step quantitative real-time qRT-PCR amplification of CHIKV genomic RNA was performed using the LightCycler®480 thermocycler (Roche Diagnostics). Five microliter of cell lysate was assayed with a final concentration of 0.4 µM of CHIKV-For and CHIKV-Rev primers each (Table 1) using the Luna® Universal One-Step RT-qPCR Kit (New England Biolabs). The relative abundance of CHIKV RNA was normalised and calculated against that of the GAPDH housekeeping gene as an endogenous reference using the 2−ΔΔCT method (86). Each sample had three independent biological replicates.

Statistical analysis: All of the analyses (unpaired Student's t-test or X^2 tests for size distribution) were performed using GraphPad Prism version 6 (GraphPad Software Inc.). *: $p<0.05$; **: $p<0.01$; ***: $p<0.001$.

Data availability: The data to support the findings of this study are included within the article.

Acknowledgments: This work was funded by the Agence Nationale de la Recherche (ANR-18-CE11-0026-01). OAP was supported by the University of Montpellier with a CBS2 doctoral school grant and by the Fondation pour la Recherche Médicale. WB was a fellow of the Méditerranée Infection, Infectiopole Sud Foundation. We are grateful to Cécile Gauthier-Rouvière and Stéphane Bodin (CRBM, Montpellier, France), Andres Merits (University of Tartu, Estonia) and Andrea Disanza (IFOM Foundation, Institute FIRC of Molecular Oncology, Milan, Italy) for sharing reagents and helpful discussions. We thank Sébastien Lyonnais (CEMIPAI, Montpellier) for valuable advice and assistance for image acquisition. We acknowledge the Montpellier RIO Imaging platform staff for technical assistance.

Authors contribution: Conceptualization: LB; Methodology: LB, WB; Investigations: OAP, WB, EB, LH, AN; Supervision: LB; Writing original draft: LB, WB, OAP. Funding acquisition: LB.

Financial disclosure statement: The funders had no role in study design, data collection and interpretation, or the decision to submit the work for publication.

References

1. Taylor MP, Koyuncu OO, Enquist LW. 2011. Subversion of the actin cytoskeleton during viral infection. 6. Nat Rev Microbiol 9:427–439.

2. Kureishy N, Sapountzi V, Prag S, Anilkumar N, Adams JC. 2002. Fascins, and their roles in cell structure and function. BioEssays 24:350–361.

3. Mattila PK, Lappalainen P. 2008. Filopodia: molecular architecture and cellular functions. 6. Nat Rev Mol Cell Biol 9:446–454.

4. Mallavarapu A, Mitchison T. 1999. Regulated Actin Cytoskeleton Assembly at Filopodium Tips Controls Their Extension and Retraction. Journal of Cell Biology 146:1097–1106.

5. Schirenbeck A, Arasada R, Bretschneider T, Stradal TEB, Schleicher M, Faix J. 2006. The bundling activity of vasodilator-stimulated phosphoprotein is required for filopodium formation. Proceedings of the National Academy of Sciences 103:7694–7699.

6. Bear JE, Svitkina TM, Krause M, Schafer DA, Loureiro JJ, Strasser GA, Maly IV, Chaga OY, Cooper JA, Borisy GG, Gertler FB. 2002. Antagonism between Ena/VASP Proteins and

527 Actin Filament Capping Regulates Fibroblast Motility. Cell 109:509–521.

528 7. Roffers-Agarwal J, Xanthos JB, Miller JR. 2005. Regulation of actin cytoskeleton
529 architecture by Eps8 and Abi1. BMC Cell Biology 6:36.

530 8. Krause M, Gautreau A. 2014. Steering cell migration: lamellipodium dynamics and the
531 regulation of directional persistence. 9. Nat Rev Mol Cell Biol 15:577–590.

532 9. Nobes CD, Hall A. 1995. Rho, Rac, and Cdc42 GTPases regulate the assembly of
533 multimolecular focal complexes associated with actin stress fibers, lamellipodia, and
534 filopodia. Cell 81:53–62.

535 10. Bustelo XR, Sauzeau V, Berenjeno IM. 2007. GTP-binding proteins of the Rho/Rac family:
536 regulation, effectors and functions in vivo. Bioessays 29:356–370.

537 11. Ridley AJ. 2006. Rho GTPases and actin dynamics in membrane protrusions and vesicle
538 trafficking. Trends in Cell Biology 16:522–529.

539 12. Hall A. 1998. Rho GTPases and the actin cytoskeleton. Science 279:509–514.

540 13. Ridley AJ, Hall A. 1992. The small GTP-binding protein rho regulates the assembly of
541 focal adhesions and actin stress fibers in response to growth factors. Cell 70:389–399.

542 14. Kurokawa K, Matsuda M. 2005. Localized RhoA Activation as a Requirement for the
543 Induction of Membrane Ruffling. MBoC 16:4294–4303.

544 15. Mullins RD, Heuser JA, Pollard TD. 1998. The interaction of Arp2/3 complex with actin:
545 Nucleation, high affinity pointed end capping, and formation of branching networks of
546 filaments. Proceedings of the National Academy of Sciences 95:6181–6186.

547 16. Czuchra A, Wu X, Meyer H, van Hengel J, Schroeder T, Geffers R, Rottner K, Brakebusch
548 C. 2005. Cdc42 Is Not Essential for Filopodium Formation, Directed Migration, Cell
549 Polarization, and Mitosis in Fibroblastoid Cells. MBoC 16:4473–4484.

550 17. Svitkina TM, Bulanova EA, Chaga OY, Vignjevic DM, Kojima S, Vasiliev JM, Borisy GG.
551 2003. Mechanism of filopodia initiation by reorganization of a dendritic network.
552 Journal of Cell Biology 160:409–421.

553 18. Laakkonen P, Auvinen P, Kujala P, Kaariainen L. 1998. Alphavirus replicase protein NSP1
554 induces filopodia and rearrangement of actin filaments. J Virol 72:10265–9.

555 19. Ahola T, Kujala P, Tuittila M, Blom T, Laakkonen P. 2000. Effects of Palmitoylation of
556 Replicase Protein nsP1 on Alphavirus Infection. Journal of Virology 74:6725–33.

557 20. Zusinaite E, Tints K, Kiiver K, Spuul P, Karo-Astover L, Merits A, Sarand I. 2007. Mutations
558 at the palmitoylation site of non-structural protein nsP1 of Semliki Forest virus
559 attenuate virus replication and cause accumulation of compensatory mutations. J Gen
560 Virol 88:1977–85.

561 21. Bartholomeeusen K, Daniel M, LaBeaud DA, Gasque P, Peeling RW, Stephenson KE, Ng

562 LFP, Ariën KK. 2023. Chikungunya fever. 1. Nat Rev Dis Primers 9:1–21.

563 22. Zaid A, Burt FJ, Liu X, Poo YS, Zandi K, Suhrbier A, Weaver SC, Texeira MM, Mahalingam
564 S. 2021. Arthritogenic alphaviruses: epidemiological and clinical perspective on
565 emerging arboviruses. The Lancet Infectious Diseases 21:e123–e133.

566 23. Khan AH, Morita K, Parquet MDC, Hasebe F, Mathenge EGM, Igarashi A. 2002. Complete
567 nucleotide sequence of chikungunya virus and evidence for an internal polyadenylation
568 site. J Gen Virol 83:3075–3084.

569 24. Strauss JH, Strauss EG. 1994. The alphaviruses: gene expression, replication, and
570 evolution. Microbiol Rev 58:491–562.

571 25. Lulla A, Lulla V, Tints K, Ahola T, Merits A. 2006. Molecular determinants of substrate
572 specificity for Semliki Forest virus nonstructural protease. J Virol 80:5413–5422.

573 26. Kril V, Aiqui-Reboul-Paviet O, Briant L, Amara A. 2021. New Insights into Chikungunya
574 Virus Infection and Pathogenesis. Annual Review of Virology.

575 27. Tan YB, Chmielewski D, Law MCY, Zhang K, He Y, Chen M, Jin J, Luo D. 2022. Molecular
576 architecture of the Chikungunya virus replication complex. Sci Adv 8:eadd2536.

577 28. Jones R, Bragagnolo G, Arranz R, Reguera J. 2020. Capping pores of alphavirus nsP1 gate
578 membranous viral replication factories. Nature.

579 29. Laurent T, Kumar P, Liese S, Zare F, Jonasson M, Carlson A, Carlson L-A. 2022.
580 Architecture of the chikungunya virus replication organelle. eLife 11:e83042.

581 30. Zhang K, Law Y-S, Law MCY, Tan YB, Wirawan M, Luo D. 2021. Structural insights into
582 viral RNA capping and plasma membrane targeting by Chikungunya virus nonstructural
583 protein 1. Cell Host Microbe 29:757-764.e3.

584 31. Jones R, Bragagnolo G, Arranz R, Reguera J. 2020. Capping pores of alphavirus nsP1 gate
585 membranous viral replication factories. Nature https://doi.org/10.1038/s41586-020-
586 3036-8.

587 32. Ahola T, Kujala P, Tuittila M, Blom T, Laakkonen P, Hinkkanen A, Auvinen P. 2000. Effects
588 of Palmitoylation of Replicase Protein nsP1 on Alphavirus Infection. Journal of Virology
589 74:6725–6733.

590 33. Spuul P, Salonen A, Merits A, Jokitalo E, Kaariainen L, Ahola T. 2007. Role of the
591 amphipathic peptide of Semliki forest virus replicase protein nsP1 in membrane
592 association and virus replication. J Virol 81:872–83.

593 34. Kallio K, Hellstrom K, Jokitalo E, Ahola T. 2015. RNA Replication and Membrane
594 Modification Require the Same Functions of Alphavirus Nonstructural Proteins. J Virol
595 90:1687–92.

596 35. Bakhache W, Neyret A, Bernard E, Merits A, Briant L. 2020. Palmitoylated Cysteines in
597 Chikungunya Virus nsP1 Are Critical for Targeting to Cholesterol-Rich Plasma Membrane

598 Microdomains with Functional Consequences for Viral Genome Replication. Journal of
599 Virology 94.

600 36. Laakkonen P, Ahola T, Kaariainen L. 1996. The effects of palmitoylation on membrane
601 association of Semliki forest virus RNA capping enzyme. J Biol Chem 271:28567–71.

602 37. Martinez MG, Kielian M. 2016. Intercellular Extensions Are Induced by the Alphavirus
603 Structural Proteins and Mediate Virus Transmission. PLOS Pathogens 12:e1006061.

604 38. Yin P, Davenport BJ, Wan JJ, Kim AS, Diamond MS, Ware BC, Tong K, Couderc T, Lecuit
605 M, Lai JR, Morrison TE, Kielian M. 2023. Chikungunya virus cell-to-cell transmission is
606 mediated by intercellular extensions in vitro and in vivo. Nat Microbiol 8:1653–1667.

607 39. Powers AM, Brault AC, Shirako Y, Strauss EG, Kang W, Strauss JH, Weaver SC. 2001.
608 Evolutionary relationships and systematics of the alphaviruses. J Virol 75:10118–31.

609 40. Kim DY, Reynaud JM, Rasalouskaya A, Akhrymuk I, Mobley JA, Frolov I, Frolova EI. 2016.
610 New World and Old World Alphaviruses Have Evolved to Exploit Different Components
611 of Stress Granules, FXR and G3BP Proteins, for Assembly of Viral Replication Complexes.
612 PLoS Pathog 12:e1005810.

613 41. Foy NJ, Akhrymuk M, Akhrymuk I, Atasheva S, Bopda-Waffo A, Frolov I, Frolova EI. 2013.
614 Hypervariable domains of nsP3 proteins of New World and Old World alphaviruses
615 mediate formation of distinct, virus-specific protein complexes. J Virol 87:1997–2010.

616 42. Peranen J, Laakkonen P, Hyvonen M, Kaariainen L. 1995. The alphavirus replicase
617 protein nsP1 is membrane-associated and has affinity to endocytic organelles. Virology
618 208:610–20.

619 43. Riedl J, Crevenna AH, Kessenbrock K, Yu JH, Neukirchen D, Bista M, Bradke F, Jenne D,
620 Holak TA, Werb Z, Sixt M, Wedlich-Soldner R. 2008. Lifeact: a versatile marker to
621 visualize F-actin. Nat Methods 5:605–607.

622 44. Leijnse N, Oddershede LB, Bendix PM. 2015. Helical buckling of actin inside filopodia
623 generates traction. Proceedings of the National Academy of Sciences 112:136–141.

624 45. Van den Broeke C, Jacob T, Favoreel HW. 2014. Rho'ing in and out of cells. Small
625 GTPases 5:e28318.

626 46. Gao Y, Dickerson JB, Guo F, Zheng J, Zheng Y. 2004. Rational design and characterization
627 of a Rac GTPase-specific small molecule inhibitor. Proceedings of the National Academy
628 of Sciences 101:7618–7623.

629 47. Surviladze Z, Waller A, Strouse JJ, Bologa C, Ursu O, Salas V, Parkinson JF, Phillips GK,
630 Romero E, Wandinger-Ness A, Sklar LA, Schroeder C, Simpson D, Nöth J, Wang J, Golden
631 J, Aubé J. 2010. A Potent and Selective Inhibitor of Cdc42 GTPaseProbe Reports from the
632 NIH Molecular Libraries Program. National Center for Biotechnology Information (US),
633 Bethesda (MD).

634 48. Uehata M, Ishizaki T, Satoh H, Ono T, Kawahara T, Morishita T, Tamakawa H, Yamagami

635 K, Inui J, Maekawa M, Narumiya S. 1997. Calcium sensitization of smooth muscle
636 mediated by a Rho-associated protein kinase in hypertension. Nature 389:990–994.

637 49. Bosco EE, Mulloy JC, Zheng Y. 2009. Rac1 GTPase: A “Rac” of All Trades. Cell Mol Life Sci
638 66:370–374.

639 50. Weernink PAO, Meletiadis K, Hommeltenberg S, Hinz M, Ishihara H, Schmidt M, Jakobs
640 KH. 2004. Activation of Type I Phosphatidylinositol 4-Phosphate 5-Kinase Isoforms by
641 the Rho GTPases, RhoA, Rac1, and Cdc42 *. Journal of Biological Chemistry 279:7840–
642 7849.

643 51. Chang K, Baginski J, Hassan SF, Volin M, Shukla D, Tiwari V. 2016. Filopodia and Viruses:
644 An Analysis of Membrane Processes in Entry Mechanisms. Front Microbiol 7:300.

645 52. Aliyu IA, Kumurya AS, Bala JA, Yahaya H, Saidu H. 2021. Proteomes, kinases and
646 signalling pathways in virus-induced filopodia, as potential antiviral therapeutics targets.
647 Rev Med Virol 31:e2202.

648 53. Jose J, Taylor AB, Kuhn RJ. 2017. Spatial and Temporal Analysis of Alphavirus Replication
649 and Assembly in Mammalian and Mosquito Cells. MBio 8.

650 54. Bernard E, Solignat M, Gay B, Chazal N, Higgs S, Devaux C, Briant L. 2010. Endocytosis of
651 Chikungunya Virus into Mammalian Cells: Role of Clathrin and Early Endosomal
652 Compartments. PLoS ONE 5.

653 55. Age Utt, Rausalu K, Jakobson M, Männik A, Alphey L, Fragkoudis R, Merits A. 2019.
654 Design and use of Chikungunya virus replication templates utilizing mammalian and
655 mosquito RNA polymerase I mediated transcription. Journal of Virology JVI.00794-19.

656 56. Birdwell CR, Strauss EG, Strauss JH. 1973. Replication of Sindbis virus: III. An electron
657 microscopic study of virus maturation using the surface replica technique. Virology
658 56:429–438.

659 57. Pavan A, Lotti LV, Torrisi MR, Migliaccio G, Bonatti S. 1987. Regional distribution of
660 Sindbis virus glycoproteins on the plasma membrane of infected baby hamster kidney
661 cells. Experimental Cell Research 168:53–62.

662 58. Ghosh A, Alladi PA, Narayanappa G, Vasanthapuram R, Desai A. 2018. The time course
663 analysis of morphological changes induced by Chikungunya virus replication in
664 mammalian and mosquito cells. av 62:360–373.

665 59. Martinez MG, Snapp EL, Perumal GS, Macaluso FP, Kielian M. 2014. Imaging the
666 alphavirus exit pathway. J Virol 88:6922–33.

667 60. Daou P, Hasan S, Breitsprecher D, Baudelet E, Camoin L, Audebert S, Goode BL, Badache
668 A. 2014. Essential and nonredundant roles for Diaphanous formins in cortical
669 microtubule capture and directed cell migration. MBoC 25:658–668.

670 61. Henty-Ridilla JL, Rankova A, Eskin JA, Kenny K, Goode BL. 2016. Accelerated actin
671 filament polymerization from microtubule plus ends. Science 352:1004–1009.

672 62. Karo-Astover L, Šarova O, Merits A, Žusinaite E. 2010. The infection of mammalian and
673 insect cells with SFV bearing nsP1 palmitoylation mutations. Virus Research 153:277–
674 287.

675 63. Nasar F, Palacios G, Gorchakov RV, Guzman H, Da Rosa APT, Savji N, Popov VL, Sherman
676 MB, Lipkin WI, Tesh RB, Weaver SC. 2012. Eilat virus, a unique alphavirus with host
677 range restricted to insects by RNA replication. Proc Natl Acad Sci U S A 109:14622–
678 14627.

679 64. Nasar F, Gorchakov RV, Tesh RB, Weaver SC. 2015. Eilat virus host range restriction is
680 present at multiple levels of the virus life cycle. J Virol 89:1404–1418.

681 65. DeRosier DJ, Edds KT. 1980. Evidence for fascin cross-links between the actin filaments
682 in coelomocyte filopodia. Exp Cell Res 126:490–494.

683 66. Krause M, Dent EW, Bear JE, Loureiro JJ, Gertler FB. 2003. Ena/VASP proteins: regulators
684 of the actin cytoskeleton and cell migration. Annu Rev Cell Dev Biol 19:541–564.

685 67. Ellis S, Mellor H. 2000. The novel Rho-family GTPase Rif regulates coordinated actin-
686 based membrane rearrangements. Current Biology 10:1387–1390.

687 68. Yang C, Svitkina T. 2011. Filopodia initiation. Cell Adhesion & Migration 5:402–408.

688 69. Van den Broeke C, Radu M, Deruelle M, Nauwynck H, Hofmann C, Jaffer ZM, Chernoff J,
689 Favoreel HW. 2009. Alphaherpesvirus US3-mediated reorganization of the actin
690 cytoskeleton is mediated by group A p21-activated kinases. Proceedings of the National
691 Academy of Sciences 106:8707–8712.

692 70. Lu X, Wu X, Plemenitas A, Yu H, Sawai ET, Abo A, Peterlin BM. 1996. CDC42 and Rac1 are
693 implicated in the activation of the Nef-associated kinase and replication of HIV-1. Curr
694 Biol 6:1677–1684.

695 71. Dadke D, Fryer BH, Golemis EA, Field J. 2003. Activation of p21-activated kinase 1-
696 nuclear factor kappaB signaling by Kaposi's sarcoma-associated herpes virus G protein-
697 coupled receptor during cellular transformation. Cancer Res 63:8837–8847.

698 72. Zamudio-Meza H, Castillo-Alvarez A, González-Bonilla C, Meza I. 2009. Cross-talk
699 between Rac1 and Cdc42 GTPases regulates formation of filopodia required for dengue
700 virus type-2 entry into HMEC-1 cells. Journal of General Virology 90:2902–2911.

701 73. Radoshitzky SR, Pegoraro G, Chī X, Dǒng L, Chiang C-Y, Jozwick L, Clester JC, Cooper CL,
702 Courier D, Langan DP, Underwood K, Kuehl KA, Sun MG, Caì Y, Yú S, Burk R, Zamani R,
703 Kota K, Kuhn JH, Bavari S. 2016. siRNA Screen Identifies Trafficking Host Factors that
704 Modulate Alphavirus Infection. PLOS Pathogens 12:e1005466.

705 74. Marei H, Malliri A. 2016. GEFs: Dual regulation of Rac1 signaling. Small GTPases 8:90–99.

706 75. Navarro-Lérida I, Sánchez-Perales S, Calvo M, Rentero C, Zheng Y, Enrich C, Del Pozo MA.
707 2012. A palmitoylation switch mechanism regulates Rac1 function and membrane
708 organization. The EMBO Journal 31:534–551.

709 76. Pohjala L, Utt A, Varjak M, Lulla A, Merits A, Ahola T, Tammela P. 2011. Inhibitors of
710 alphavirus entry and replication identified with a stable Chikungunya replicon cell line
711 and virus-based assays. PLoS ONE 6:e28923.

712 77. Spuul P, Balistreri G, Kaariainen L, Ahola T. 2010. Phosphatidylinositol 3-kinase-, actin-,
713 and microtubule-dependent transport of Semliki Forest Virus replication complexes
714 from the plasma membrane to modified lysosomes. J Virol 84:7543–57.

715 78. Gorchakov R, Garmashova N, Frolova E, Frolov I. 2008. Different types of nsP3-
716 containing protein complexes in Sindbis virus-infected cells. J Virol 82:10088–101.

717 79. Frolova E, Gorchakov R, Garmashova N, Atasheva S, Vergara LA, Frolov I. 2006.
718 Formation of nsP3-specific protein complexes during Sindbis virus replication. J Virol
719 80:4122–34.

720 80. Barton DJ, Sawicki SG, Sawicki DL. 1991. Solubilization and immunoprecipitation of
721 alphavirus replication complexes. J Virol 65:1496–506.

722 81. Mutso M, Morro AM, Smedberg C, Kasvandik S, Aquilimeba M, Teppor M, Tarve L, Lulla
723 A, Lulla V, Saul S, Thaa B, McInerney GM, Merits A, Varjak M. 2018. Mutation of CD2AP
724 and SH3KBP1 Binding Motif in Alphavirus nsP3 Hypervariable Domain Results in
725 Attenuated Virus. Viruses 10.

726 82. Zhang N, Zhao H, Zhang L. 2019. Fatty Acid Synthase Promotes the Palmitoylation of
727 Chikungunya Virus nsP1. Journal of Virology 93:e01747-18.

728 83. Kummerer BM, Grywna K, Glasker S, Wieseler J, Drosten C. 2012. Construction of an
729 infectious Chikungunya virus cDNA clone and stable insertion of mCherry reporter genes
730 at two different sites. J Gen Virol 93:1991–5.

731 84. Utt A, Rausalu K, Jakobson M, Männik A, Alphey L, Fragkoudis R, Merits A. 2019. Design
732 and Use of Chikungunya Virus Replication Templates Utilizing Mammalian and Mosquito
733 RNA Polymerase I-Mediated Transcription. Journal of Virology 93:10.1128/jvi.00794-19.

734 85. Disanza A, Mantoani S, Hertzog M, Gerboth S, Frittoli E, Steffen A, Berhoerster K,
735 Kreienkamp H-J, Milanesi F, Fiore PPD, Ciliberto A, Stradal TEB, Scita G. 2006. Regulation
736 of cell shape by Cdc42 is mediated by the synergic actin-bundling activity of the Eps8–
737 IRSp53 complex. 12. Nat Cell Biol 8:1337–1347.

738 86. Livak KJ, Schmittgen TD. 2001. Analysis of Relative Gene Expression Data Using Real-
739 Time Quantitative PCR and the 2−ΔΔCT Method. Methods 25:402–408.

740

741 **Figure legends**

742 **Figure 1**: **CHIKV nsP1 significantly reshapes the cell membranes**. (A) HEK293T or HeLa cells were
743 infected for 16h with the CHIKV-m377 virus for 16 h, labelled antibodies against nsP1 and DAPI, and
744 then processed for confocal imaging. Virus replication sites were detected using anti-dsRNA
745 antibodies. Filopodia and lamellipodia formed at the cell surface are indicated by white and red
746 arrows respectively. Inset are enlarged and colocalized signals are indicated (yellow arrows). Phase
747 contrats image of non infected (NI) HEK293T is shown as control. (B) HEK293T cells expressing the
748 native nsP1 protein, detected using specific antibodies, or expressing the indicated fusion proteins
749 were analyzed by confocal microscopy. A phase-contrast image of cells cxpressing the GFP-nsP1
750 protein is shown. (C & D) Still images video of cells transfected with GFP-nsP1 showing the dynamic
751 of filopodia-like extensions (C) and lamellipodia (D). In D, filopodia growing from lamellipodia are
752 indicated by a white arrow and retracting ruffles with persisting fibers attached to the substrate are
753 shown by a red arrow. The number (E) and length (F) of filopodia-like extensions formed in CHIKV-
754 infected cells and in cells expressing GFP, GFP-nsP1 and GFP-nsP1$_{AAA}$ were quantified, each dots
755 representing an independent cell ($n \geq 8$). Results are representative of 3 independent experiments.

756 **Figure 2: nsP1 membrane deformation capacity is conserved across evolution in human-relevant**
757 **alphavirus.** (A) Confocal imaging of HeLa cells expressing nsP1 encoded by CHIKV, SFV, SINV, VEEV
758 and EILV fused with GFP. Nuclei were stained with DAPI. Scale bar: 10µm. (B) Filopodia numbers
759 were quantified from at least 8 cells (A). Results are representative of 3 independent experiments.
760 (C) Amino acid sequence alignment of nsP1 from alphavirus in this study. Conservation of
761 palmitoylated cysteines is indicated in boldface.

762 **Figure 3**: **Contribution of actin cytoskeleton in nsP1-induced membrane extensions**. HeLa cells
763 transfected with GFP or GFP-nsP1 were either (A) cotransfected with the CMV-LifeAct-TagRFP
764 plasmid to visualize cellular actin, or (B) labelled with anti-tubulin mAbs. Nuclei were stained with
765 DAPI. Colocalized fluorescences are shown by arrows and Pearson's coefficient determined from the

region of interest are indicated. Scale bar: 10 µm. (C) Pearson's coefficient quantifying colocalization of GFP-nsP1 with actin or tubulin. Each value corresponds to a region of interest determined from 9 cells for actin and from 11 cells for tubulin. (D)Time-lapse microscopy of HEK293T cells expressing GFP-nsP1 and CMV-LifeAct-TagRFP. The frames display the position changes of filopodia over time (indicted in seconds). Colocalized actin and nsP1 fluorescences in filopodia and in lamellipodia are indicated by white arrows and green arrows respectively. (E) Confocal imaging of cells expressing the GFP-nsP1 protein incubated for 4 hrs in the presence of 0.25 µM cytochalasin D (CytoD), 0.1 µM nocodazole (NoD), or vehicle (Mock). (F) Number of filopodia per cell was determined from >15 cells in (C), each dot representing an independent cell. Results are representative of 3 independent experiments.

Figure 4: Presence of filopodia markers fascin, Eps8 and VASP on nsP1-induced cell extensions. HeLa cells expressing an untagged nsP1 were cotransfected with plasmids encoding either Eps8-GFP, VASP-GFP, or fascin-GFP proteins as indicated. After 24 hrs the cells were labelled with anti-nsP1 antibodies and processed for confocal imaging. Nuclei were stained with DAPI. Scale bar: 10 µm.

Figure 5: Rac1 GTPase is critical for nsP1-induced membrane protrusions. (A) Schematic representation of Rho GTPase-dependent actin regulation in filopodia and lamellipodia formation. Inhibitors used in this study are indicated (created with Biorender.com). (B) HeLa cells transfected to express GFP-nsP1 were cultured in the presence of vehicle (Mock), NSC23766 (100 µM), ML-141 (20 µM) or Y-27632 (20 µM) for 24 hrs before analysis by confocal microscopy. Nuclei are stained with DAPI. Scale bar: 10 µm. For each condition, filopodia number (C) and length (D) were determined from >20 cells. (E) Cells transfected with siRNA against Rac1 (siRac1) or a non-targeting control (siCtrl) were analyzed for Rac1 and GAPDH expression. Rac1 expression level determined using GAPDH as an internal control is indicated for each condition. (F) Then the cells were transfected to express GFP-nsP1 and processed for confocal microscopy after 24 hrs. Nuclei were stained with DAPI. Filopodia count (G) and length (H) were determined from >20 cells, each dots representing an

independent cell. (I) HEK293T cells were cotransfected to express the untagged nsP1 together with either a GFP-tagged Rac1 protein (GFP-$Rac1_{WT}$) or a Rac1 dominant negative mutant (GFP-$Rac1_{N17}$). The cells were processed as above. Results are representative of 3 independent experiments.

Figure 6: PAK1 and Arp2 effectors of Rac1 are pivotal in nsP1-induced membrane deformation. (A) HEK293T cells were transfected with non-targetting siRNA or siRNA targeting Arp2, PAK1, IQGAP and PIP5K1 for 48 hrs and with siRNA targeting IRSp53 for 72 hrs. Knockdown efficiency was controlled by immunoblotting. Host protein expression level was determined by densitometry scanning using GAPDH as an internal control. Values normalized to 1 for the control condition are indicated for each condition. (B) Then, the cells were transfected to express GFP-nsP1, stained with DAPI and analyzed by confocal microscopy. Filopodia count per cell (C) and extension length (D) were determined from >25 cells in (B), each dots representing an independent cell. Results are representative of 3 independent experiments.

Figure 7: Rac1 GTPase activity is required for CHIKV infection. HEK293T cells were infected with a CHIKV-Luc reporter virus for 1 hr (MOI 1) and then incubated with increasing concentrations of GTPase inhibitor added to the culture medium 1 hr before (A) or after (C) the viral challenge. After 6 hrs in culture, infection was determined by quantifying luciferase activity in the cell lysates (histograms). Drug toxicity was determined using uninfected cells maintained under similar conditions for the duration of the experiment (dotted line). Results represent the mean of triplicates. The experimental design is depicted above each histogram. (B and D) Cells maintained with medium alone (black dots) or medium supplemented with 25 µM NSC23766 (white dots) added 1h before (B) or after (D) CHIKV challenge were subjected to qRT-PCR quantification of viral RNA at 3, 6 and 8 hrs post-infection. Values represent mean of triplicates and are representative of 3 independent experiments.

Figure 8: **Rac1 and its downstream effectors PAK1 and Arp2 are required for CHIKV genome replication.** (A) HEK293T cells transfected with the CHIKV transreplication system were incubated

816 with the indicated concentrations of NSC23766. Genome replication was determined by
817 quantification of cell-associated luciferase activity. Cell viability is indicated for each condition
818 (dotted line). (B) Expression of nsP1 in mock-treated cells and in cells maintained in the presence of
819 75 µM NSC23766 (NSC) was determined by immunoblot. NsP1 expression level determined using
820 actin as internal control is indicated. (C) Genome replication was evaluated as in (A) in cells
821 expressing the GFP-tagged $Rac1_{WT}$ or $Rac1_{N17}$ GTPases or the control GFP protein. (D-F) Cells
822 transfected with siRNA against Rac1 (D), PAK1 (E), or Arp2 (F), or with a non-targetting control (siCtrl)
823 for 48 hrs were analyzed for target protein expression by immunoblot. Relative band intensity
824 normalized according to actin level is indicated. The cells were then transfected with the CHIKV
825 transreplication system, and genome replication was determined after 24 hrs by quantification of
826 luciferase activity in the cell lysate. All values represent the mean of triplicates and are
827 representative of 3 independent experiments.

828 **Table 1: Primer and siRNA sequences**

PCR primers	
$nsP1_{SINV}$-Fw	5’- TTTCACTCGAGccATGGAGAAGCCAGTAGTAAAC
$nsP1_{SINV}$-Rev	5’- GTTTCGGGCCCTTATGCTCCGATGTCCGCCTGGA
$nsP1_{SFV}$-Fw	5’-CGAAGCTCGAGCCATGGCCGCCAAAGTGCAT
$nsP1_{SFV}$-Rev	5’-TCCACGGGCCCTGCACCTGCGTGATACTC
$nsP1_{VEEV}$-Fw	5’- GGCTTCCTCGAGCCATGGAGAAAGTTCACGTTG
$nsP1_{VEEV}$-Rev	5’- GTCTCGGGCCCTTAGGCCCCAGCCTCTTGTAAC
$nsP1_{EILV}$-Fw	5’- ACAGATCTCGAGccATGGAGAAACCAACTGTTAAC
$nsP1_{EILV}$-Rev	5’- GGTCTGGGCCCTTACCCGCCGATGTCGTCGGAG
CHIKV-Fw	5’-GGCAGTGGTCCCAGATAATTCAA
CHIKV-Rev	5’-GCTGTCTAGATCCACCCCATACA
GAPDH-For	5’-GCTCACCGGCATGGCCTTTCGCGT
GAPDH-Rev	5’-TGGAGGAGTGGGTGTCGCTGTTGA
siRNA	
Rac1	5’- GAACAGAACUGCUAUUUCCUCUAAU
Arp2	5’- GGGUAACAAUGGGUGGUCUUCUGAU
PAK1	5’- GGAUGAAGGCCAAAUUGCAGCUGUG
IRSp53	5’- AUGGGGAAGAAUUACGAGAAGGCAC
IQGAP	5’- GGUUGCAGUACUAUAUUGUAAGCTT
PPP5K1	5’- GCCAGGCUAUAGUAAUUAUUACUAT
Non-targeting	5’-GAAGAACUGCUAUUUCCUCUAAAU

829

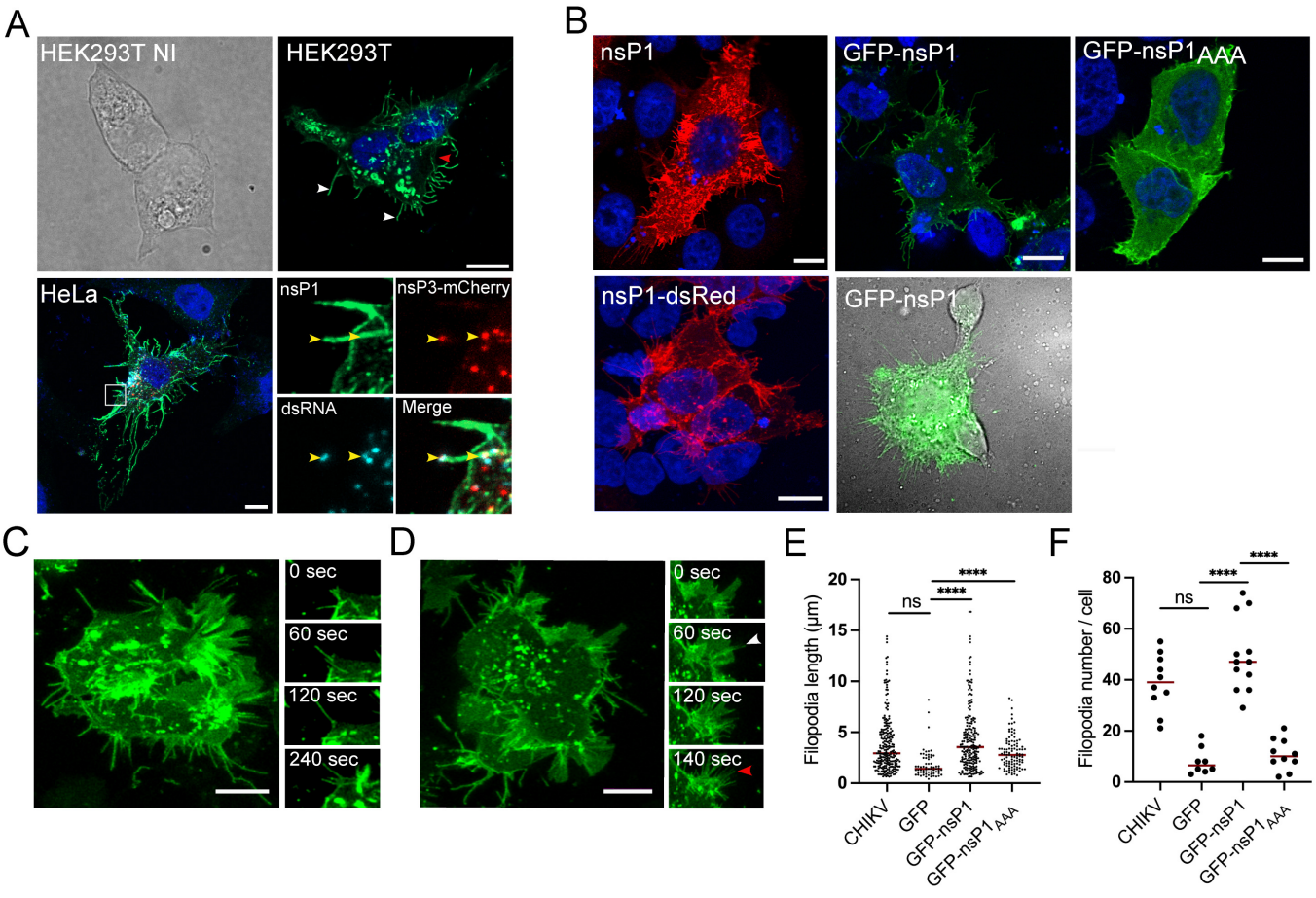
A
HEK293T NI
HEK293T
HeLa
nsP1
nsP3-mCherry
dsRNA
Merge
B
nsP1
GFP-nsP1
GFP-nsP1AAA
nsP1-dsRed
GFP-nsP1
C
0 sec
60 sec
120 sec
240 sec
D
0 sec
60 sec
120 sec
140 sec
E
Filopodia length (µm)
ns
****
****
CHIKV
GFP
GFP-nsP1
GFP-nsP1AAA
F
Filopodia number / cell
ns
****
****
CHIKV
GFP
GFP-nsP1
GFP-nsP1AAA

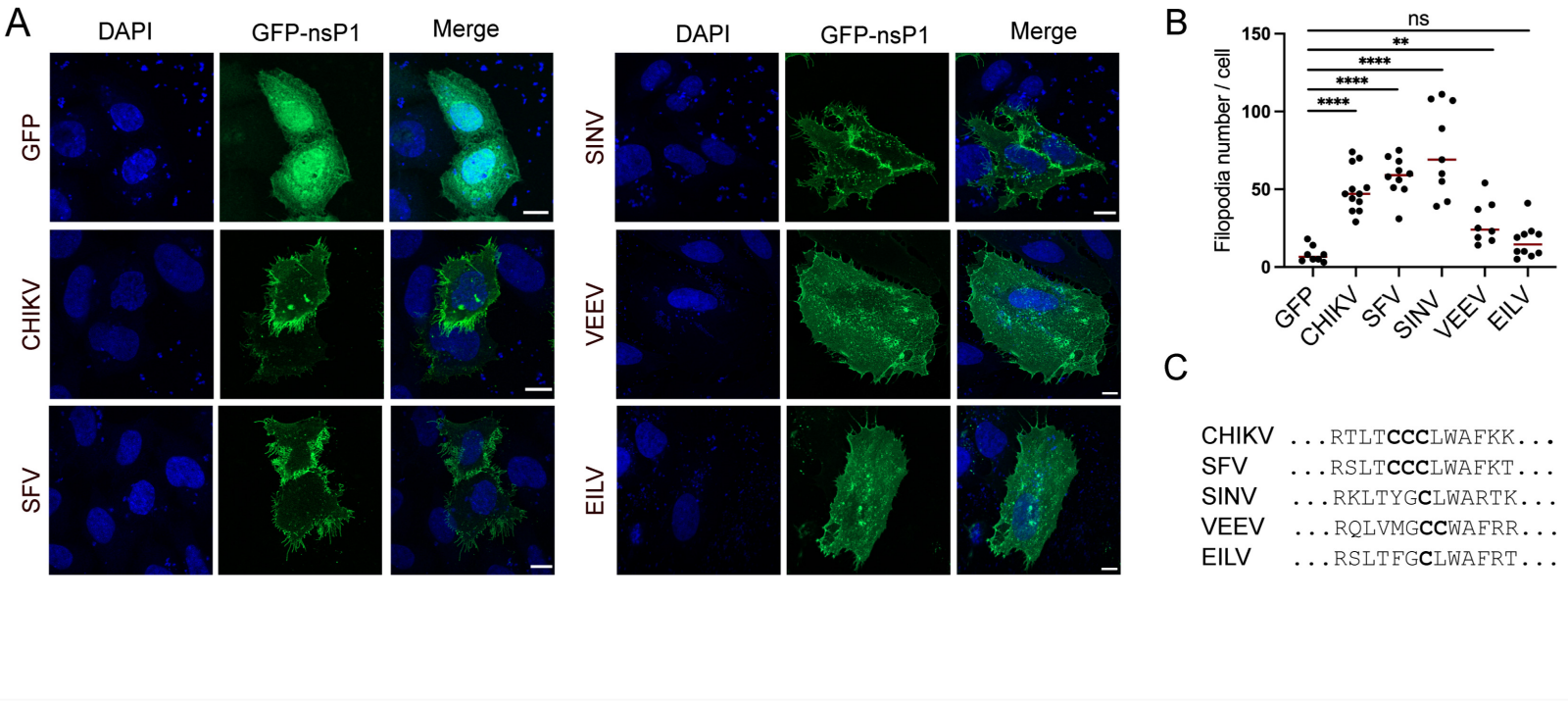
A
DAPI
GFP-nsP1
Merge
GFP
CHIKV
SFV
SINV
VEEV
EILV
B
Filopodia number / cell
150
100
50
0
ns
**
****
****
****
GFP
CHIKV
SFV
SINV
VEEV
EILV
C
CHIKV ...RTLTCCCLWAFKK...
SFV ...RSLTCCCLWAFKT...
SINV ...RKLTYGCLWARTK...
VEEV ...RQLVMGCCWAFRR...
EILV ...RSLTFGCLWAFRT...

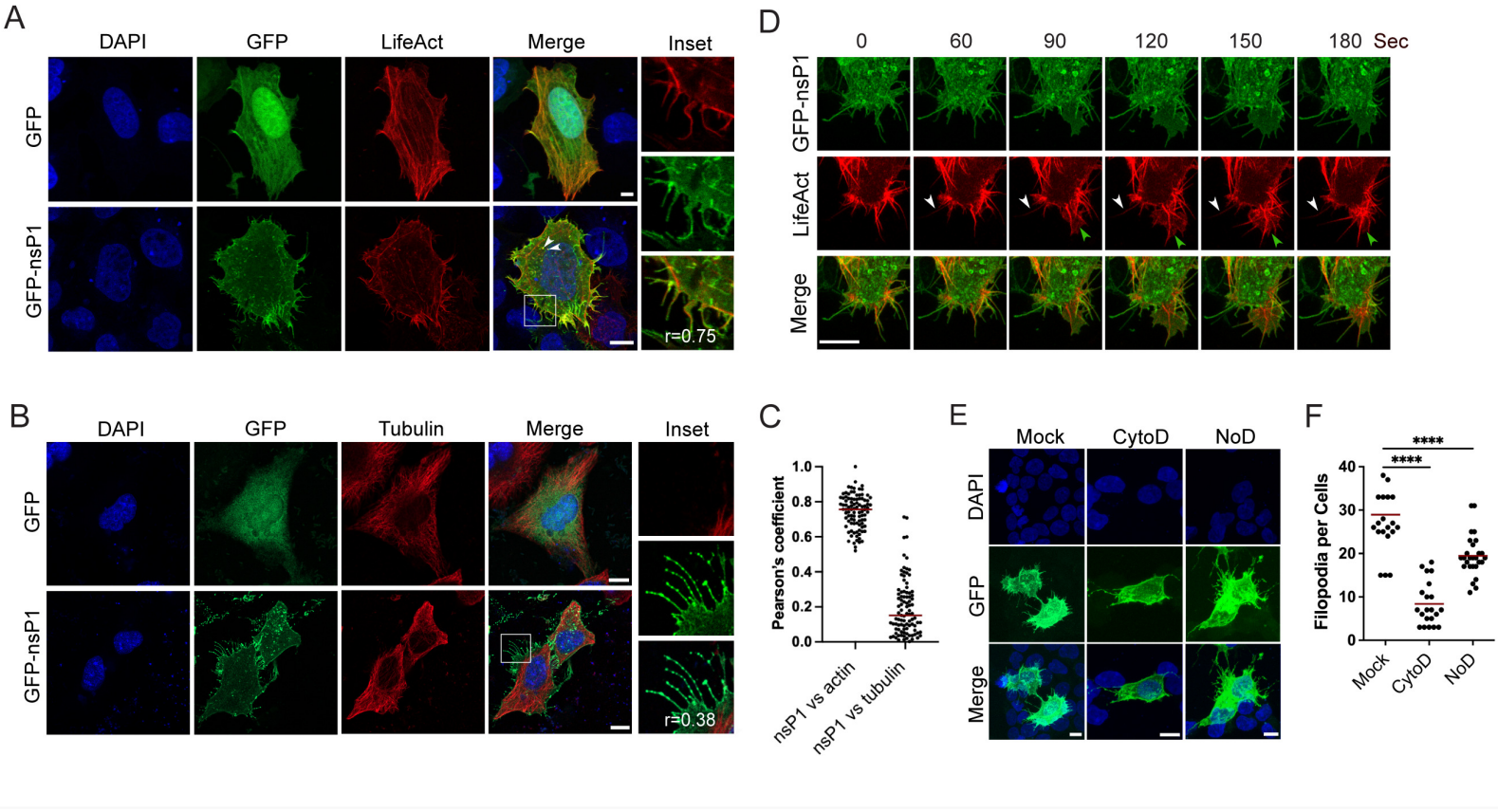
A
DAPI
GFP
LifeAct
Merge
Inset
GFP
GFP-nsP1
r=0.75
D
0
60
90
120
150
180 Sec
GFP-nsP1
LifeAct
Merge
B
DAPI
GFP
Tubulin
Merge
Inset
GFP
GFP-nsP1
r=0.38
C
Pearson's coefficient
1.0
0.8
0.6
0.4
0.2
0.0
nsP1 vs actin
nsP1 vs tubulin
E
Mock
CytoD
NoD
DAPI
GFP
Merge
F
Filopodia per Cells
40
30
20
10
0
****
****
Mock
CytoD
NoD

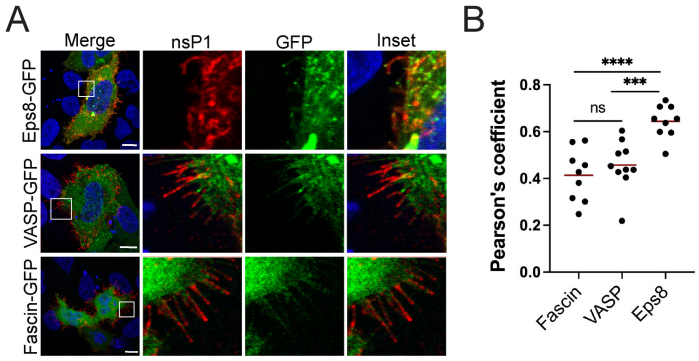
A
Merge
nsP1
GFP
Inset
Eps8-GFP
VASP-GFP
Fascin-GFP
B
Pearson's coefficient
0.0
0.2
0.4
0.6
0.8
ns
***
****
Fascin
VASP
Eps8

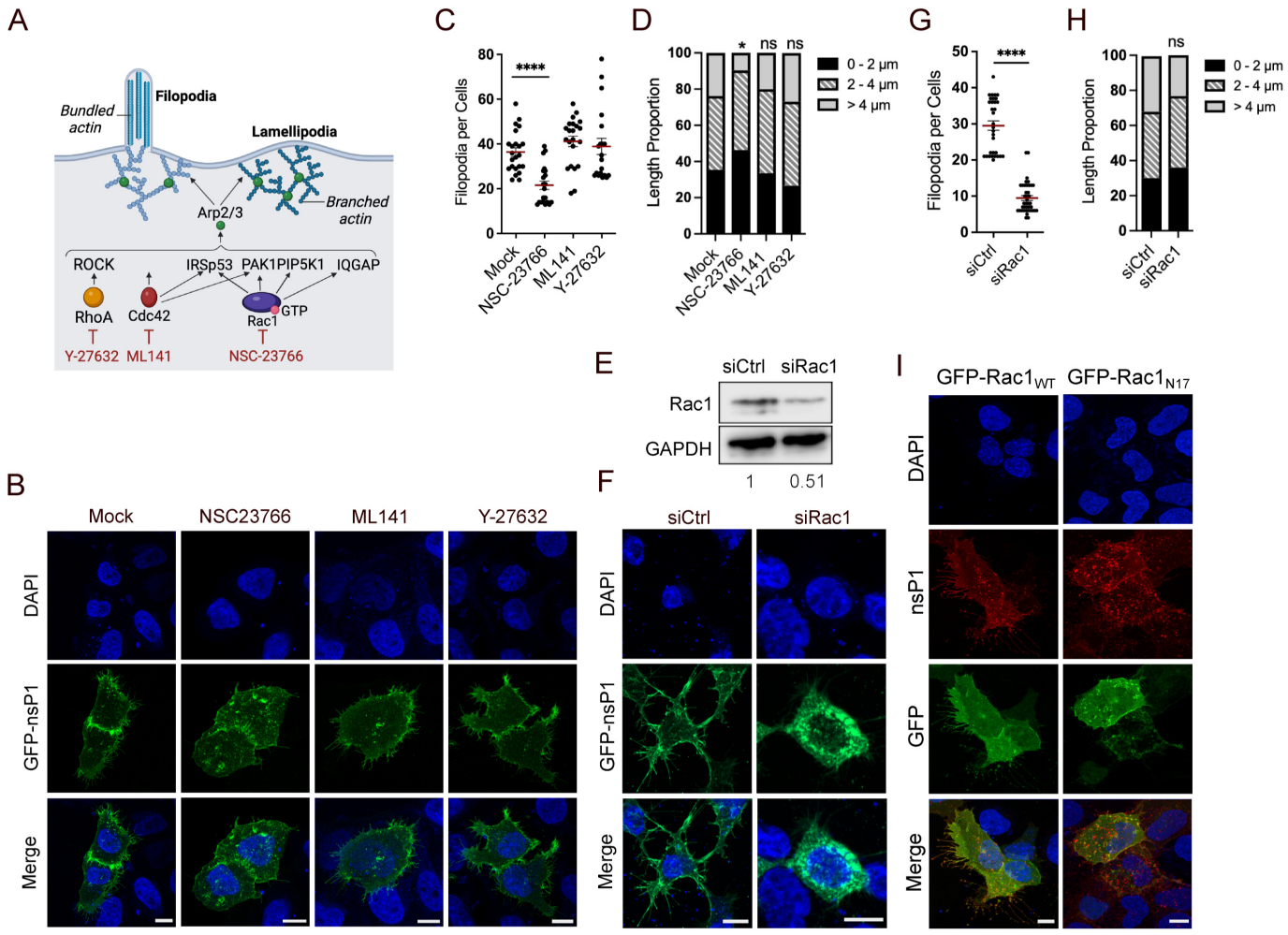
A
Bundled actin
Filopodia
Lamellipodia
Arp2/3
Branched actin
ROCK
IRSp53
PAK1PIP5K1
IQGAP
RhoA
Cdc42
Rac1
GTP
Y-27632
ML141
NSC-23766
C
Filopodia per Cells
****
Mock
NSC-23766
ML141
Y-27632
D
Length Proportion
*
ns
ns
0 - 2 µm
2 - 4 µm
> 4 µm
G
Filopodia per Cells
****
siCtrl
siRac1
H
Length Proportion
ns
E
siCtrl
siRac1
Rac1
GAPDH
1
0.51
B
Mock
NSC23766
ML141
Y-27632
DAPI
GFP-nsP1
Merge
F
siCtrl
siRac1
I
GFP-Rac1WT
GFP-Rac1N17
DAPI
nsP1
GFP
Merge

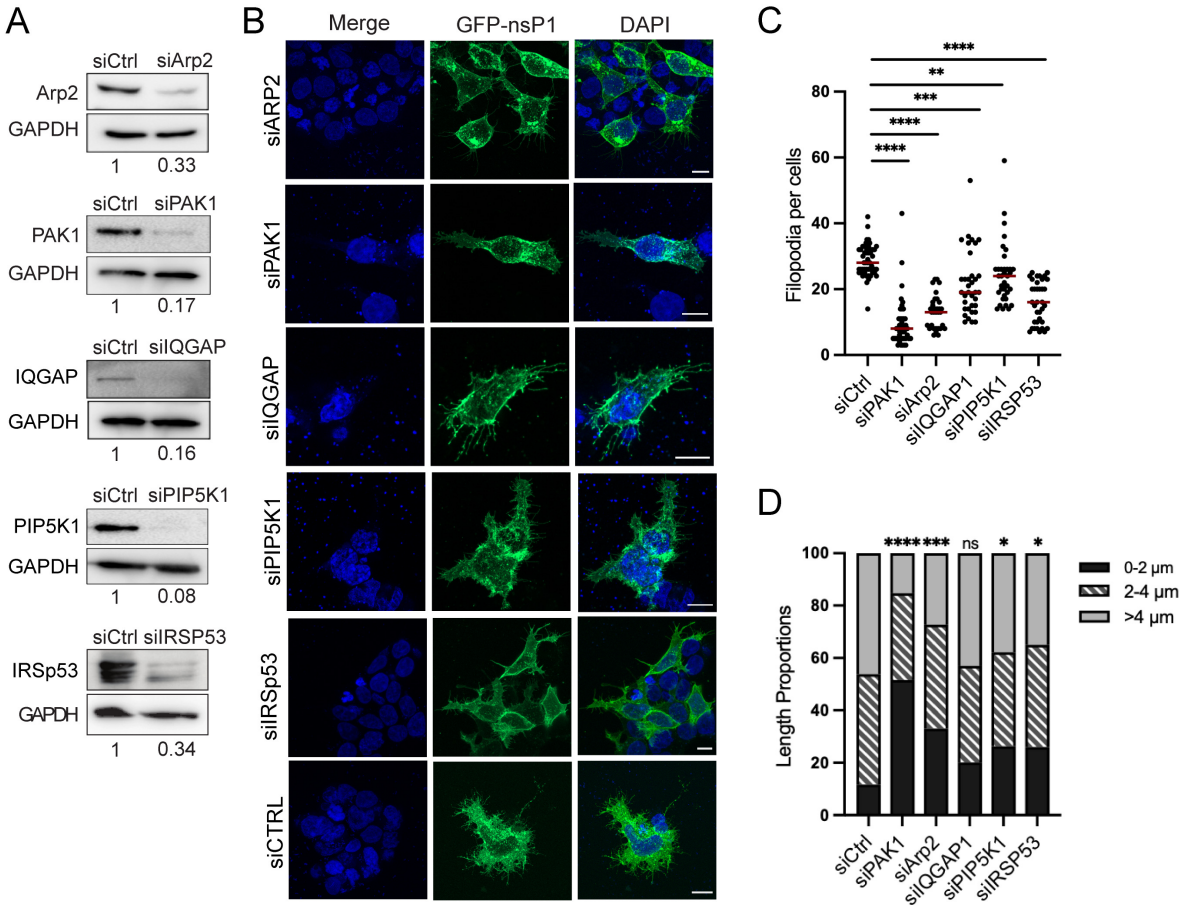
A
siCtrl siArp2
Arp2
GAPDH
1 0.33
siCtrl siPAK1
PAK1
GAPDH
1 0.17
siCtrl siIQGAP
IQGAP
GAPDH
1 0.16
siCtrl siPIP5K1
PIP5K1
GAPDH
1 0.08
siCtrl siIRSP53
IRSp53
GAPDH
1 0.34
B
Merge
GFP-nsP1
DAPI
siARP2
siPAK1
siIQGAP
siPIP5K1
siIRSp53
siCTRL
C
Filopodia per cells
0
20
40
60
80
****
**
***
****
****
siCtrl
siPAK1
siArp2
siIQGAP1
siPIP5K1
siIRSP53
D
Length Proportions
0
20
40
60
80
100
****
****
ns
*
*
0-2 µm
2-4 µm
>4 µm
siCtrl
siPAK1
siArp2
siIQGAP1
siPIP5K1
siIRSP53

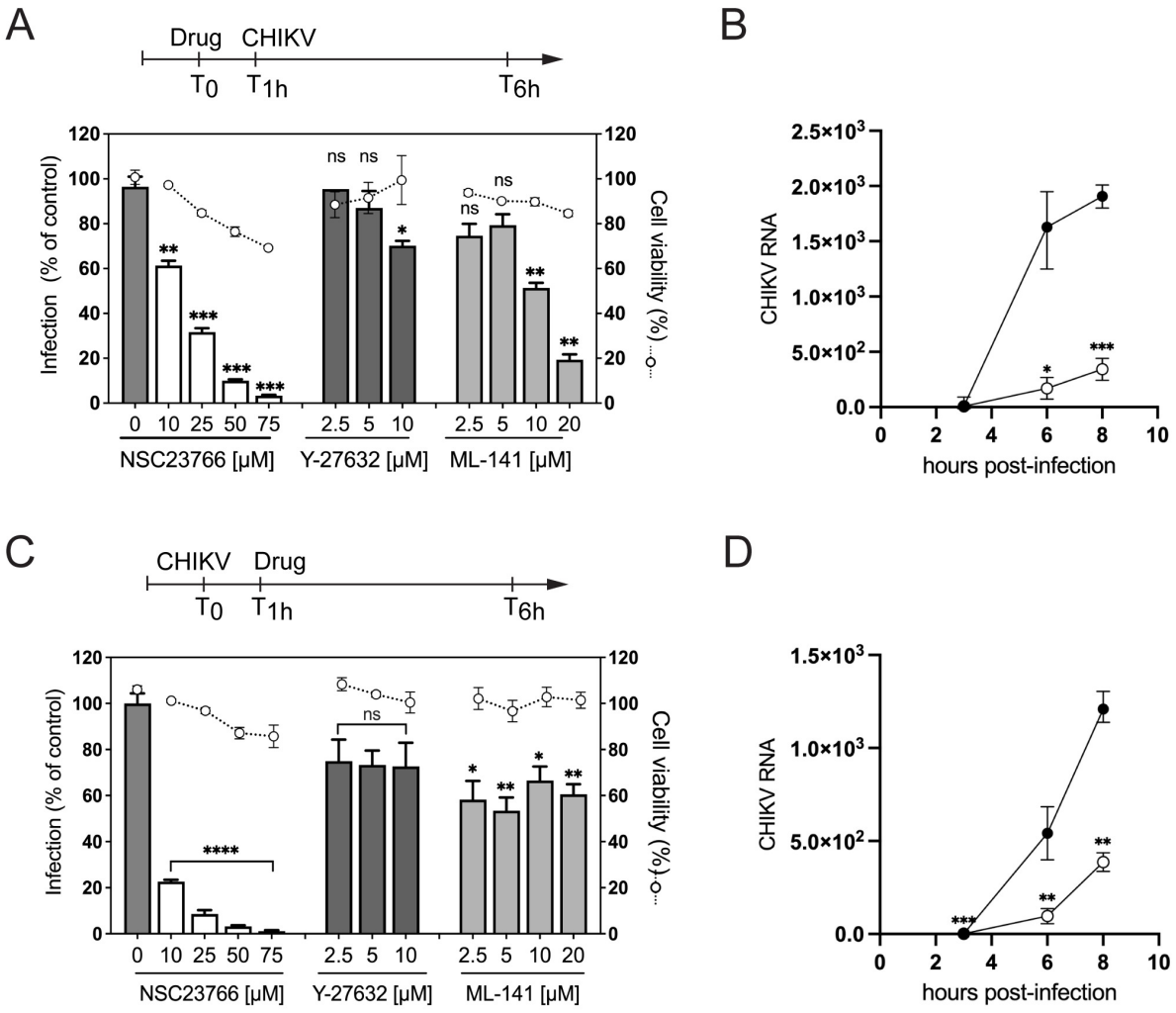
A
Drug
CHIKV
T0
T1h
T6h
Infection (% of control)
Cell viability (%)
NSC23766 [μM]
Y-27632 [μM]
ML-141 [μM]
B
CHIKV RNA
hours post-infection
C
CHIKV
Drug
T0
T1h
T6h
Infection (% of control)
Cell viability (%)
NSC23766 [μM]
Y-27632 [μM]
ML-141 [μM]
D
CHIKV RNA
hours post-infection

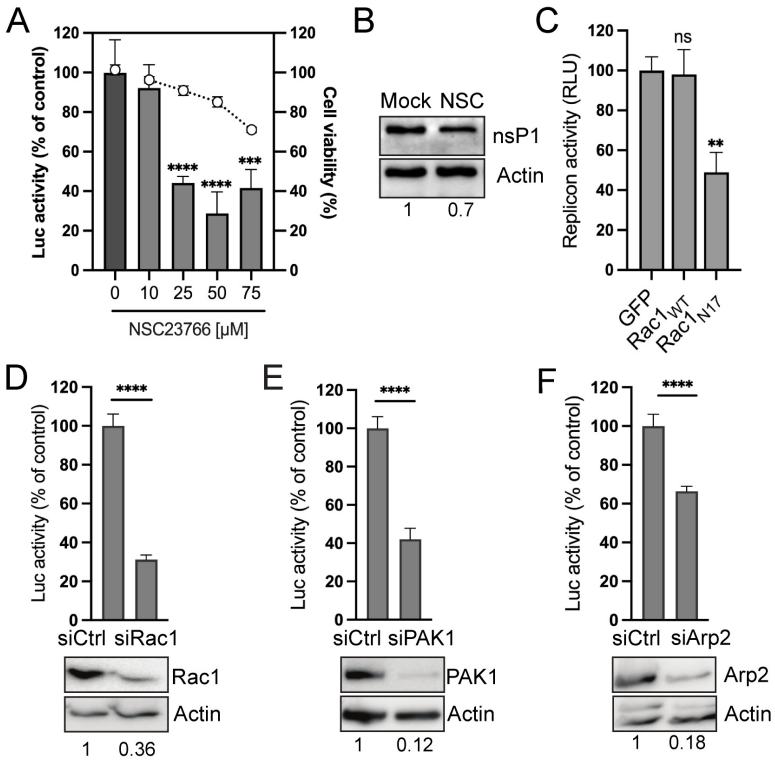
A
Luc activity (% of control)
Cell viability (%)
120
100
80
60
40
20
0
****
****
***
0 10 25 50 75
NSC23766 [μM]
B
Mock NSC
nsP1
Actin
1 0.7
C
Replicon activity (RLU)
ns
**
GFP
Rac1WT
Rac1N17
D
Luc activity (% of control)
****
siCtrl siRac1
Rac1
Actin
1 0.36
E
Luc activity (% of control)
****
siCtrl siPAK1
PAK1
Actin
1 0.12
F
Luc activity (% of control)
****
siCtrl siArp2
Arp2
Actin
1 0.18